JOC The Journal of Organic Chemistry

Article

pubs.acs.org/joc

Methyl [^{13}C]Glucopyranosiduronic Acids: Effect of COOH Ionization and Exocyclic Structure on NMR Spin-Couplings

Wenhui Zhang,[†] Xiaosong Hu,[†,‡] Ian Carmichael,[§] and Anthony S. Serianni*[,†]

[†]Department of Chemistry and Biochemistry and [§]The Radiation Laboratory, University of Notre Dame, Notre Dame, Indiana 46556-5670, United States

Supporting Information

ABSTRACT: Methyl α- and β-D-glucopyranuronides singly labeled with ^{13}C at C1−C6 were prepared from the corresponding ^{13}C-labeled methyl D-glucopyranosides, and multiple NMR J-couplings (J_{HH}, J_{CH}, and J_{CC}) were measured in their protonated and ionized forms in aqueous (^2H_2O) solution. Solvated density functional theory (DFT) calculations of J-couplings in structurally related model compounds were performed to determine how well the calculated J-couplings matched the experimental values in saccharides bearing an ionizable substituent. Intraring J_{HH} values in both uronide anomers, including $^3J_{H4,H5}$, are unaffected by solution pD, and COOH ionization exerts little effect on J_{CH} and J_{CC} except for $^1J_{C1,H1}$, $^1J_{C4,H4}$, $^1J_{C5,H5}$, $^1J_{C5,C6}$, and $^2J_{C3,C5}$, where changes of up to 5 Hz were observed. Some of these changes are associated with changes in bond lengths upon ionization; in general, better agreement between theory and experiment was observed for couplings less sensitive to exocyclic C−O bond conformation. Titration of ^{1}H and ^{13}C chemical shifts, and some J-couplings, yielded a COOH pK_a of 3.0 ± 0.1 in both anomers. DFT calculations suggest that substituents proximal to the exocyclic COOH group (i.e., the C4−O4 bond) influence the activation barrier to C5−C6 bond rotation due to transient intramolecular H-bonding. A comparison of J-couplings in the glucopyranuronides to corresponding J-couplings in the glucopyranosides showed that more pervasive changes occur upon conversion from a COOH to a CH_2OH substituent at C6 than from COOH ionization within the uronides. Twelve J-couplings are affected, with the largest being $^1J_{C5,C6}$ (~18 Hz larger in the uronides), followed by $^2J_{C6,H5}$ (~2.5 Hz more negative in the uronides).

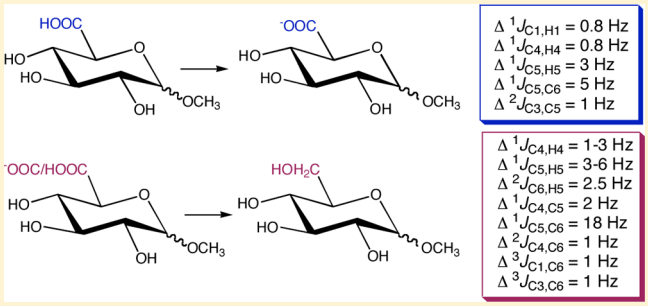

INTRODUCTION

D-Glucuronic acid (GlcUA) is a major monosaccharide constituent of glycosaminoglycans (GAGs) such as hyaluronic acid (HA) and chondroitin sulfate.[1] In these high molecular weight mucopolysaccharides, GlcUA is part of a disaccharide repeating unit **1** comprised of a β-D-glucopyranuronosyl residue 1→3-linked to a 2-acetamido-2-deoxy-β-D-glucopyranosyl (GlcNAc) or 2-acetamido-2-deoxy-β-D-galactopyranosyl (GalNAc) residue, the latter in turn 1→3-linked to the β-D-glucopyranuronosyl residue in the following unit.[2] The GlcNAc or GalNAc residues may be *O*-sulfated, which along with the COO^- groups give the polysaccharide significant negative charge at physiological pH. GAGs play diverse roles in biological systems.[3] For example, hyaluronic acid is distributed widely in connective, epithelial, and neural tissues of vertebrates, is a major component of the vitreous humor of the eye,[4] and is one of the major components of the extracellular matrix. HA contributes to cell proliferation and migration and has been implicated in the progression of some malignant tumors.[5]

Glucuronidation involves the covalent attachment of GlcUA residues to specific biomolecules *in vivo* to give a GlcUA conjugate, which renders toxic substances harmless and more water-soluble, and allows for their subsequent elimination via excretion.[6] This process involves the sugar nucleotide donor, UDP-D-glucuronic acid (UDP-GlcUA), and a family of UDP-glucuronosyltransferases that catalyze the transfer of GlcUA from UDP-GlcUA to different molecular targets. UDP-GlcUA also serves as the metabolic precursor in the biosynthesis of ascorbic acid (vitamin C) in mammals able to synthesize this vitamin.[7] Glucuronic acid is often linked to drugs to promote drug delivery.[8]

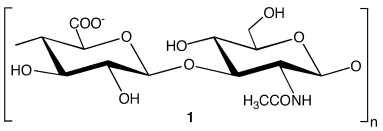

1

Herein we describe high-resolution ^{1}H and ^{13}C NMR studies of methyl α- and β-D-glucopyranuronides **2** and **3** selectively labeled with ^{13}C at each of their six carbons. The aims of this investigation, which extend earlier work[9,10] on chemical shifts within glucuronic acid, were 3-fold: (1) to determine a full set of J_{HH}, J_{CH} and J_{CC} spin-couplings in the methyl glycosides of GlcUA in their protonated ($\mathbf{2}^p$, $\mathbf{3}^p$) and ionized ($\mathbf{2}^i$, $\mathbf{3}^i$) states;

Received: May 31, 2012
Published: September 11, 2012

   dx.doi.org/10.1021/jo3011182 | J. Org. Chem. 2012, 77, 9521−9534

(2) to quantify the effect of C6 oxidation on *J*-coupling behavior in aldohexopyranosyl rings through comparisons of *J*-couplings in **2** and **3** with those in methyl α- (**4**) and β- (**5**) D-glucopyranosides; and (3) to determine the degree to which *J*-couplings calculated from density functional theory (DFT) in **2** and **3** agree with corresponding experimental values in protonated and ionized forms. The latter aim extends recent work on *N*-acetyl-neuraminic acid **6** in which similar comparisons of DFT-derived *J*-couplings to experimental values were reported.[11] The results of this investigation contribute to the longer-range goal of establishing reliable relationships between the magnitudes and signs of trans-glycoside *J*-couplings and glycoside linkage conformation in oligosaccharides[12−14] containing ionizable residues.

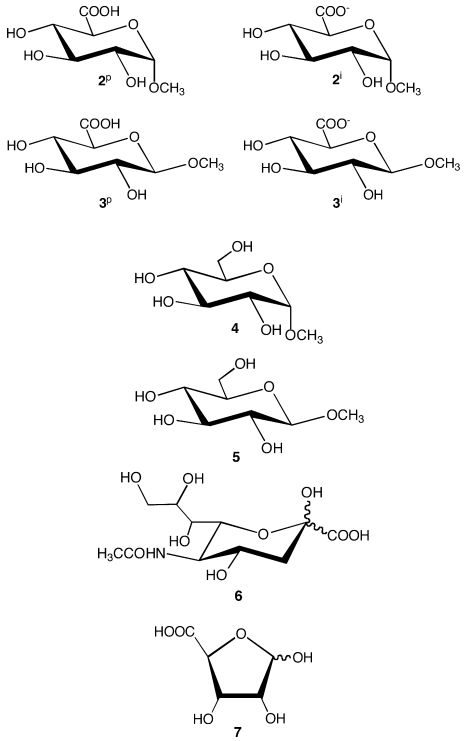

RESULTS AND DISCUSSION

A. ^{1}H and ^{13}C Chemical Shifts in 2 and 3. ^{1}H and ^{13}C chemical shifts for **2** and **3** at pD 1.3−1.4 and 7.0 are shown in Table 1 (see Tables S1 and S2 for δ_H and δ_C over the pD range 1−7, Supporting Information). Representative ^{1}H and ^{13}C NMR spectra of **2**^{p} and **3**^{p} are shown in Figures 1−4.

The effect of increasing solution pD from 1 to 7 on δ_{H2}, δ_{H3} and $\delta_{OC\underline{H}_3}$ in **2** and **3** is small (downfield shifts of ≤0.03 ppm). In contrast, δ_{H1} and δ_{H4} shift upfield by 0.01−0.06 ppm with increasing pD, while δ_{H5} shifts upfield by ∼0.25 ppm; the magnitudes of these changes depend inversely on proximity to the site of ionization.

The effect of solution pD on ^{13}C chemical shifts decreases in the following order: $\delta_{C6} > \delta_{C5} > \delta_{C4} > \delta_{C3} \approx \delta_{C2} \approx \delta_{C1} \approx \delta_{OCH_3}$ (Figure 5). Signals from C2, C3, C4, C5 and C6 shift downfield with increasing pD, whereas those of C1 and OCH_3 shift upfield (Table 1; Figure 5). These chemical shift changes mimic those reported for D-riburonic acid **7**,[15] although their magnitudes differ; for example, the change in δ_{C6} is considerably greater than that in δ_{C5} in **2**/**3** (∼3.6 ppm vs ∼1.5 ppm, respectively; Figure 5), whereas changes in the related δ_{C4} and δ_{C5} in **7** are comparable (overall 3−3.8 ppm).

Table 1. ^{1}H and ^{13}C Chemical Shifts[a] for 2 and 3 at pD 1.3−1.4 and 7.0

pD	δ_{H1}	δ_{H2}	δ_{H3}	δ_{H4}	δ_{H5}	δ_{OMe}
			methyl α-D-glucopyranosiduronic acid **2**			
1.4	4.816	3.567	3.652	3.528	4.117	3.390
7.0	4.793	3.577	3.655	3.473	3.867	3.400
			methyl β-D-glucopyranosiduronic acid **3**			
1.3	4.362	3.248	3.458	3.511	3.943	3.486
7.0	4.349	3.273	3.480	3.478	3.686	3.540
pD	δ_{C1}	δ_{C2}	δ_{C3}	δ_{C4}	δ_{C5}	δ_{C6}	δ_{OMe}
			methyl α-D-glucopyranosiduronic acid **2**				
1.4	102.22	73.42	75.27	73.97	73.10	175.66	58.19
7.0	101.97	73.70	75.53	74.62	74.57	179.24	57.84
			methyl β-D-glucopyranosiduronic acid **3**				
1.3	105.77	75.16	77.76	73.71	76.87	174.63	59.92
7.0	105.63	75.44	78.12	74.32	78.47	178.31	59.76

[a]In ppm in ^2H_2O at 30 °C; ± 0.01 ppm for ^{13}C, ± 0.001 ppm for ^{1}H. ^{1}H and ^{13}C data for **2** were obtained using methyl α-D-[6-^{13}C]-glucopyranuronic acid. ^{1}H Data for **3** were obtained using methyl β-D-[3-^{13}C], [4-^{13}C] and [6-^{13}C]glucopyranuronic acids, and ^{13}C data were obtained using methyl β-D-[6-^{13}C]glucopyranuronic acid. Chemical shifts were referenced externally to sodium 4,4-dimethyl-4-silapentane-1-sulfonate (DSS).

B. Energetics and Effects of C5−C6 Bond Rotation on Bond Lengths in 2_c and 3_c. DFT Calculations were undertaken to examine the effects of rotating ω and θ on the energies of 2_c and 3_c, and on specific bond lengths ($r_{C5,C6}$, $r_{C5,O5}$, $r_{C5,H5}$ and $r_{C4,C5}$) in these structures. These results, which shed light on the conformational properties of exocyclic COOH groups in saccharides and on potential structural factors that influence NMR *J*-couplings, are discussed in the Supporting Information. Here the discussion focuses exclusively on the experimental *J*-couplings measured in **2** and **3** and on the comparison of these experimental values to calculated couplings derived from DFT.

C. ^{1}H−^{1}H Spin-Coupling Constants. The large $^3J_{H2,H3}$, $^3J_{H3,H4}$ and $^3J_{H4,H5}$ in **2** and **3** (9.0 − 10.0 Hz) (Table 2) are consistent with *trans* arrangements between the coupled hydrogens, and indicate preferred $^4C_1$ ring conformations in both structures in ^2H_2O solution. These $^3J_{HH}$ are essentially unaffected by anomeric configuration, although $^3J_{H2,H3}$ is consistently larger in **2** than in **3** by ∼0.4 Hz. J_{HH} in **2** and **3** are unaffected by COOH ionization state, including $^3J_{H4,H5}$.

Calculated ^{1}H−^{1}H spin-couplings (Table 2) are in good agreement with the experimental couplings, deviating by less than ±0.4 Hz in most cases; computed $^3J_{H2,H3}$ in **2** show the greatest deviation from experiment (0.7 Hz). A comparison of experimental J_{HH} values in the methyl D-glucopyranosides **4** and **5** to corresponding values in **2** and **3** shows that substitution of a CH_2OH group at C6 with a COOH group results in essentially no change in intraring J_{HH}.

D. ^{13}C−^{1}H Spin-Coupling Constants. *1. One-Bond Couplings.* $^1J_{C1,H1}$ depends on anomeric configuration, with coupling for the equatorial C1−H1 bond in **2** ∼9 Hz larger than coupling for the axial C1−H1 bond in **3** (Table 3).[19,20] The equatorial bond is expected to be shorter than the axial bond, with the resulting enhanced *s*-character producing the larger $^1J_{CH}$.[21] $^1J_{C1,H1}$ is relatively insensitive to COOH ionization state (<1 Hz change) and to structure at C6

dx.doi.org/10.1021/jo3011182 | J. Org. Chem. 2012, 77, 9521−9534

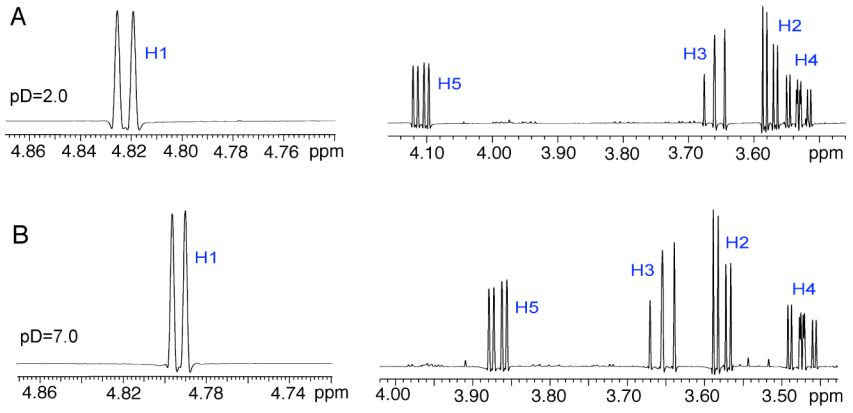

Figure 1. ^{1}H NMR spectra (600 MHz) at 30 °C of [6-^{13}C]**2** in $^{2}H_2O$ at pD 2.0 (A) and pD 7.0 (B). The additional splitting of the H4 and H5 signals is due to $^{3}J_{C6,H4}$ and $^{2}J_{C6,H5}$, respectively.

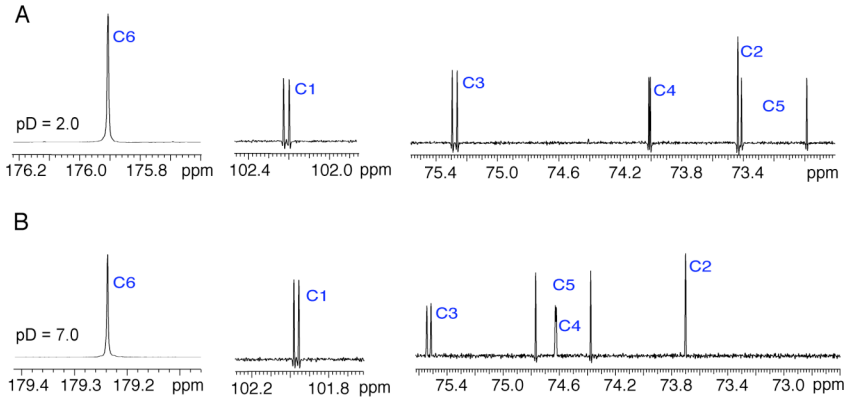

Figure 2. ^{13}C NMR spectra (150 MHz) at 30 °C of [6-^{13}C]**2** in $^{2}H_2O$ at pD 2.0 (A) and pD 7.0 (B). All signals of unlabeled carbons except C2 are doublets due to ^{13}C−^{13}C spin-coupling to C6.

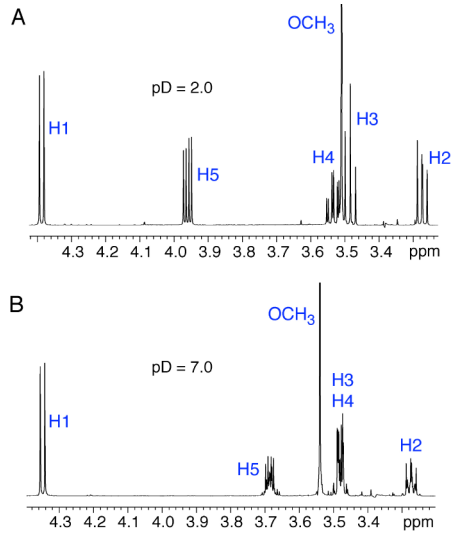

Figure 3. ^{1}H NMR spectra (600 MHz) at 30 °C of [6-^{13}C]**3** in $^{2}H_2O$ at pD 2.0 (A) and pD 7.0 (B). The additional splitting of the H4 and H5 signals is due to $^{3}J_{C6,H4}$ and $^{2}J_{C6,H5}$, respectively. Virtual coupling in the H2 and H5 signals in (B) is caused by the coincident and mutually coupled H3 and H4 signals. This overlap is removed in ^{1}H spectra of [3-^{13}C]**3** and [4-^{13}C]**3**, thereby allowing direct measurement of δ and J-values without the need for simulation (see Figures S16 and S17, Supporting Information).

(COOH vs CH_2OH). Calculated $^{1}J_{C1,H1}$ in $\mathbf{2}_c$ and $\mathbf{3}_c$ are in fair agreement with experiment; differences range from 1.1 Hz ($\mathbf{2}^i$) to 6.9 Hz ($\mathbf{3}^p$). $^{1}J_{C1,H1}$ in all four forms shows a moderate dependence on ω; an effect of θ is also discernible in $\mathbf{3}_c^i$ but is negligible in $\mathbf{2}_c^p$, $\mathbf{3}_c^p$ and $\mathbf{2}_c^i$ (Figure S1, Supporting Information). COOH ionization reduces calculated $^{1}J_{C1,H1}$ values more than is observed experimentally (for $\mathbf{2}_c$, $\Delta \approx 5$ Hz; for $\mathbf{3}_c$, $\Delta \approx 3$ Hz); the experimental differences are 0.8 and 0.9 Hz, respectively (Table 3).

$^{1}J_{C2,H2}$ and $^{1}J_{C3,H3}$ in **2** and **3** are ∼20 Hz smaller than $^{1}J_{C1,H1}$ and are unaffected by the COOH ionization state. $^{1}J_{C2,H2}$ is unaffected by anomeric configuration, but $^{1}J_{C3,H3}$ appears smaller in **3** than in **2** by ∼2.6 Hz in both the protonated and ionized forms. $^{1}J_{C2,H2}$ and $^{1}J_{C3,H3}$ in **2** and **3** are similar to the corresponding couplings in methyl glucopyranosides **4** and **5**.

$^{1}J_{C4,H4}$ and $^{1}J_{C5,H5}$ in **2** and **3** depend on COOH ionization state, with smaller couplings observed in the ionized state in both cases (reduction of ∼1 Hz for $^{1}J_{C4,H4}$; ∼2.8 Hz for $^{1}J_{C5,H5}$). $^{1}J_{C4,H4}$ and $^{1}J_{C5,H5}$ are larger in **2**/**3** than in the corresponding aldohexopyranosides (increase of 1−3 Hz for $^{1}J_{C4,H4}$; 3−6 Hz for $^{1}J_{C5,H5}$).

Calculated $^{1}J_{C5,H5}$ values are in better agreement with experiment than calculated $^{1}J_{C2,H2}$, $^{1}J_{C3,H3}$ and $^{1}J_{C4,H4}$. This behavior is attributed in part to an improper accounting of the effects of C2−O2, C3−O3 and C4−O4 bond conformation on calculated $^{1}J_{CH}$; conformational averaging of vicinal lone-pair (Perlin) effects on C−H bond length[22] affects these couplings in solution. This effect is absent for $^{1}J_{C5,H5}$ since O5 is in a fixed orientation with respect to the C5−H5 bond. The influence of ω on $^{1}J_{C5,H5}$ was therefore examined, since changes in $r_{C5,H5}$

dx.doi.org/10.1021/jo3011182 | J. Org. Chem. 2012, 77, 9521−9534

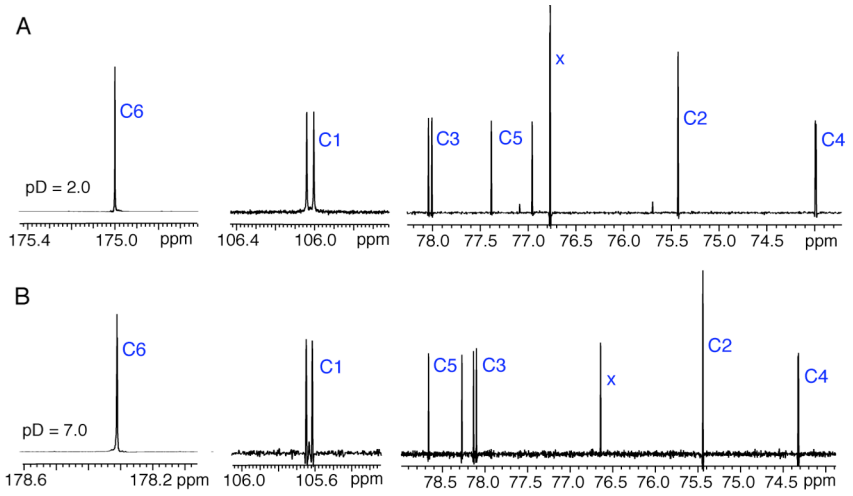

Figure 4. ^{13}C NMR spectra (150 MHz) at 30 °C of [6-^{13}C]**3** in $^{2}H_2O$ at pD 2.0 (A) and at pD 7.0 (B). All signals of unlabeled carbons except C2 are doublets due to $^{13}C-^{13}C$ coupling to C6. Signal "x" is an unidentified impurity.

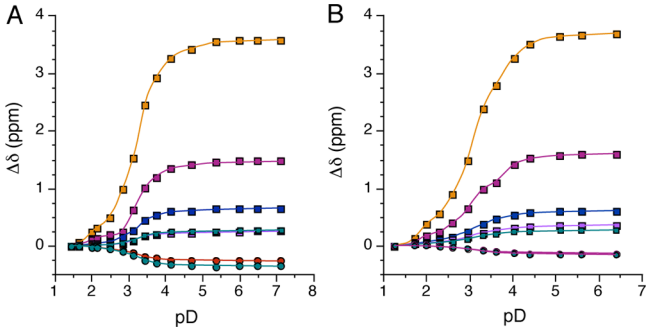

Figure 5. ^{13}C Chemical shift titration curves for **2** (A) and **3** (B). $\Delta\delta = \delta$ (higher pH) $- \delta$ (lowest pH), with positive values indicating downfield shifts. C1, red circles; C2, green squares; C3, lavender squares; C4, blue squares; C5, pink squares; C6, yellow squares; OCH_3, green circles. Lines were generated by interpolation.

Table 2. Experimental J_{HH}[a] in 2 and 3 at pD 2.0 and 7.0, and Calculated J_{HH}[b] in 2_c^p, 2_c^i, 3_c^p and 3_c^i

	2		3	
J_{HH} (Hz)	pD 2.0	pD 7.0	pD 2.0	pD 7.0
$^3J_{H1,H2}$	3.8 (**4.1**; *3.8*)	3.8 (**4.2**)	8.0 (**7.6**; *8.0*)	8.0 (**7.8**)
$^3J_{H2,H3}$	9.7 (**9.0**; *9.8*)	9.8 (**9.1**)	9.3 (**8.8**; *9.5*)	9.4 (**9.0**)
$^3J_{H3,H4}$	9.0 (**8.7**; *9.2*)	9.0 (**8.7**)	9.1 (**8.7**; *9.2*)	9.0 (**8.8**)
$^3J_{H4,H5}$	10.0(**9.9**; *10.0*)	10.0 (**9.9**)	9.9 (**9.8**; *10.0*)	9.9 (**9.9**)

[a]Experimental values (30 °C, ^2H_2O; ± 0.1 Hz) are shown in normal text. [b]Calculated values (in bold) were obtained by averaging the full data set of calculated couplings (12 values of ω × 3 fixed values of θ = 36 couplings) (see Calculational Methods). Experimental values in **4** and **5** are shown in italics (taken from ref 16).

with ω (Figure S2, Supporting Information) might result in changes in $^1J_{C5,H5}$. As shown in Figure 6 for 2_c^i and 3_c^i, $^1J_{C5,H5}$ depends on ω and to a lesser extent on θ. The curves are bimodal and symmetric as expected, with maximal coupling observed at 60°/240° or 90°/270°, and minimal coupling observed at 150°/300° or 0°/180°. Maximal $^1J_{C5,H5}$ thus correlate with shorter $r_{C5,H5}$. In both 2_c^i and 3_c^i, a 30° shift is observed in the curve when $\theta = -60°$, possibly caused by H-bonding between O4H (donor) and the carboxylate anion (acceptor) at ω of 0° and 180°. This interaction apparently reduces $^1J_{C5,H5}$ relative to those couplings in structures lacking this interaction. Related plots for 2_c^p and 3_c^p are dissymmetric and show an irregular dependence of $^1J_{C5,H5}$ on ω; the 0°-180° regions are similar to those shown in Figure 6, but the 180°-360° regions are relatively flat (i.e., devoid of the second defined maximum) (data not shown).

2. Two-Bond Couplings. $^2J_{CCH}$ for coupling pathways remote from the COOH group in **2** and **3** (i.e., $^2J_{C1,H2}$, $^2J_{C2,H1}$, $^2J_{C2,H3}$) are unaffected by COOH ionization and are identical to corresponding couplings in **4** and **5** (Table 4). $^2J_{CH}$ for coupling pathways proximal to the COOH group (i.e., $^2J_{C4,H3}$, $^2J_{C4,H5}$, $^2J_{C5,H4}$, $^2J_{C6,H5}$) become less negative upon COOH ionization and deviate significantly from corresponding couplings in **4** and **5**. The largest differences between **2**/**3** and **4**/**5** are observed for $^2J_{C6,H5}$, which is more negative by ~2.5 Hz in **2**/**3** than in **4**/**5**. The substitution of COOH for CH_2OH at C6 does not affect proximal $^2J_{CH}$ in the same fashion; for example, $^2J_{C4,H5}$ and $^2J_{C6,H5}$ become more negative, whereas $^2J_{C5,H4}$ becomes less negative. The behaviors of $^2J_{C3,H2}$ and $^2J_{C3,H4}$ are less systematic; both are unaffected by COOH ionization, but only $^2J_{C3,H4}$ in **3** differs appreciably from the corresponding coupling in **5**. The latter difference could be caused by different C2−O2, C3−O3 and/or C4−O4 bond conformations in solution in **2**/**3** and **4**/**5**, structural factors known to affect the magnitudes of $^2J_{CCH}$ in vicinal diol fragments, especially when the rotated C−O bond is attached to the carbon bearing the coupled hydrogen.[23]

Like **4**/**5**,[14] internal $^2J_{CH}$ values in **2** and **3** depend on anomeric configuration. $^2J_{C3,H2}$ is considerably more negative in **2** than in **3** at pD 2.0 and pD 7.0; the *anti* orientation of O1 relative to H2 in **2** results in the more negative value (1,2-*trans* "remote effect"[18]). $^2J_{C3,H4}$ and $^2J_{C4,H3}$ are unaffected by anomeric configuration in **4** and **5** but depend on anomeric configuration in **2** and **3**; the reason for this difference remains obscure.[19,20]

Calculated $^2J_{CH}$ are only in fair agreement with experimental couplings, presumably because of inadequate modeling of exocyclic C−O bond rotamers in the calculations (see similar argument above on errors in calculated $^1J_{CH}$). Calculated $^2J_{CH}$ provide information on coupling sign; in all cases except $^2J_{C1,H2}$ and $^2J_{C2,H1}$ in **2**, the experimental $^2J_{CH}$ are predicted to be negative. While most $^2J_{CH}$ in 2_c and 3_c are insensitive to ω

dx.doi.org/10.1021/jo3011182 | J. Org. Chem. 2012, 77, 9521−9534

Table 3. Experimental $^1J_{CH}$[a] in 2 and 3 at pD 2.0 and 7.0, and Calculated $^1J_{CH}$[b] in 2_c^P, 2_c^i, 3_c^P and 3_c^i

	2			3		
J_{CH} (Hz)	pD 2.0	pD 7.0	Me α-Glcp **4**	pD 2.0	pD 7.0	Me β-Glcp **5**
$^1J_{C1,H1}$	171.4 (176.6)	170.6 (171.7)	170.1	162.4 (169.3)	**161.5** (165.8)	161.3
$^1J_{C2,H2}$	145.7 (149.9)	145.5 (148.3)	~145.9	145.5 (152.1)	**145.3** (150.9)	145.0
$^1J_{C3,H3}$	**146.0** (151.3)	146.2 (149.1)	146.5	143.6 (148.2)	143.3 (146.3)	142.9
$^1J_{C4,H4}$	146.0 (151.5)	145.2 (149.1)	144.4	147.8 (151.9)	146.8 (149.8)	144.8
$^1J_{C5,H5}$	150.3 (151.9)	147.7 (147.4)	144.3	147.2 (149.8)	**144.2** (145.0)	141.8

[a]At 30 °C in ^2H_2O; ± 0.1 Hz. Couplings shown in bold were obtained by spectral simulation using MacNuts software.[17] [b]Calculated J_{CH} (in parentheses) were obtained by averaging the full data set of calculated couplings (12 values of ω × 3 fixed values of θ = 36 couplings) (see Calculational Methods). Couplings in **4** and **5** were taken from previous work.[16,18]

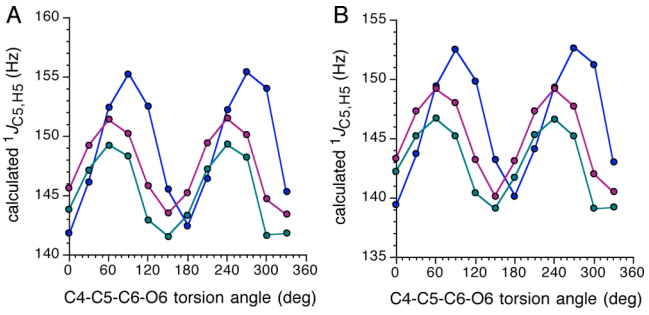

Figure 6. Effect of C5−C6 bond rotation (ω) on calculated $^1J_{C5,H5}$ in 2_c^i (A) and 3_c^i (B). Green, θ = 60°; red, θ = 180°; blue, θ = −60°.

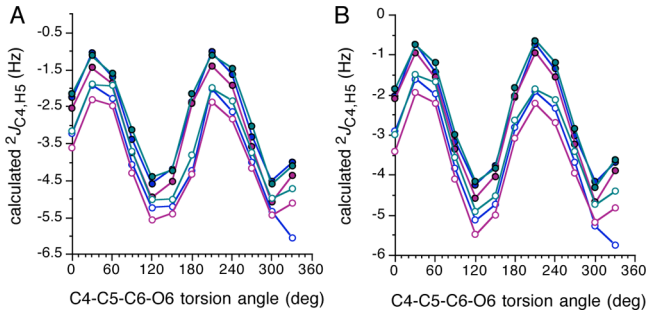

Figure 7. Effect of C5−C6 bond rotation (ω) on the calculated $^2J_{C4,H5}$ in (A) 2_c and (B) 3_c. Open symbols, 2_c^P and 3_c^P. Filled symbols, 2_c^i and 3_c^i. Green, θ = 60°; red, θ = 180°; blue, θ = −60°.

(data not shown), $^2J_{C4,H5}$ shows a strong dependence (Figure 7). In both anomers of **2** and **3** in their protonated and ionized forms, $^2J_{C4,H5}$ is least negative for ω of ~30° and 210°, and most negative for ω of 120° and 300°, with an overall change at each value of θ of ~3 Hz. The data show a small shift to less negative couplings in the ionized forms, in qualitative agreement with experiment (Table 4). $^2J_{C6,H5}$ also shows a dependence on ω, although the overall change at each θ is more modest (~1.5 Hz) than observed for $^2J_{C4,H5}$ (Figure S3, Supporting Information). Phase shifting is observed in the curve for θ = −60°, similar to observations made on $^1J_{C5,H5}$ (Figure 6); as proposed for $^1J_{C5,H5}$, H-bonding between O4H (donor) and the carboxylate (acceptor) is probably responsible for this behavior.

3. Three-bond Couplings. Vicinal $^3J_{CH}$ values in **2** and **3** (Table 5) are essentially unaffected by COOH ionization state, including $^3J_{C6,H4}$, with differences of 0.3 Hz or less. Experimental $^3J_{CH}$ in **2**/**3** are nearly identical to corresponding couplings in **4**/**5**, with the exception of $^3J_{C6,H4}$, which is ~1 Hz smaller in the uronides. $^3J_{CCCH}$ involving ring carbons fall into two categories, those corresponding to *gauche* and those corresponding to *anti* C−C−C−H torsion angles. The former yields values of ~1 Hz, and the latter yields values of ~5 Hz. $^3J_{CH}$ involving the ring oxygen displays different behavior, with *gauche* couplings of 1−2 Hz and *anti* couplings of ~6.5 Hz. Substitution of carbon by the more electronegative oxygen within the coupling pathway appears to increase coupling by ~1 Hz, although different torsion angles may also contribute to the differences. As found in **4**/**5**,[18] $^3J_{C3,H5}$ in **2** and **3** (2.2−2.7 Hz) are ~1.5 Hz larger than expected, suggesting that this coupling pathway possesses unique intrinsic properties

Table 4. Experimental $^2J_{CH}$[a] in 2 and 3 at pD 2.0 and 7.0, and Calculated $^2J_{CH}$[b] in 2_c^P, 2_c^i, 3_c^P and 3_c^i

	2			3		
J_{CH} (Hz)	pD 2.0	pD 7.0	Me α-Glcp **4**	pD 2.0	pD 7.0	Me β-Glcp **5**
$^2J_{C1,H2}$	0.9 (3.2)	0.9 (3.0)	+1.0	6.3 (−4.7)	**6.3** (−4.5)	−6.3
$^2J_{C2,H1}$	~1.1 (0.4)	~1.3 (0.2)	*~1.1*	0 (1.4)	0 (1.7)	0
$^2J_{C2,H3}$	5.6 (−3.1)	5.5 (−3.2)	−5.5	4.4 (−3.2)	**4.3** (−3.2)	−4.3
$^2J_{C3,H2}$	5.8 (−4.5)	6.0 (−4.6)	−6.2	4.6 (−4.2)	4.5 (−4.1)	−4.2
$^2J_{C3,H4}$	**4.1** (−3.9)	**4.2** (−3.5)	−4.3	5.1 (−3.9)	4.9 (−3.5)	−4.2
$^2J_{C4,H3}$	**4.4** (−4.2)	4.1 (−4.3)	−4.7	5.4 (−4.4)	5.3 (−4.4)	−4.8
$^2J_{C4,H5}$	**4.0** (−3.8)	3.7 (−2.9)	−2.9	3.7 (−3.4)	3.1 (−2.6)	−2.9
$^2J_{C5,H4}$	3.4 (−2.6)	3.0 (−2.6)	−3.9	3.4 (−2.9)	3.4 (−2.8)	−4.0
$^2J_{C6,H5}$	4.4 (−3.2)	3.9 (−2.7)	−1.4	4.7 (−3.6)	4.2 (−2.9)	−2.2

[a]At 30 °C in ^2H_2O; ± 0.1 Hz. Coupling constants in bold were obtained by spectral simulation using MacNuts software.[17] Values in italic were measured at 300 MHz in [2-^{13}C]**4** during the present work. [b]Calculated J_{CH} (in parentheses) were obtained by averaging the full data set of calculated couplings (12 values of ω × 3 fixed values of θ = 36 couplings) (see Calculational Methods). Couplings shown for **4** and **5** were taken from previous work.[16,18]

dx.doi.org/10.1021/jo3011182 | J. Org. Chem. 2012, 77, 9521−9534

Table 5. Experimental $^3J_{CH}$[a] in 2 and 3 at pD 2.0 and 7.0 and Calculated $^3J_{CH}$[b] in 2_c^p, 2_c^i, 3_c^p and 3_c^i

	2			3		
J_{CH} (Hz)	pD 2.0	pD 7.0	Me α-Glc*p* **4**	pD 2.0	pD 7.0	Me β-Glc*p* **5**
$^3J_{C1,H3}$	~0 (0.9)	~0 (0.9)	~0	1.1 (1.3)	**1.0** (1.3)	1.2
$^3J_{C1,H5}$	1.6 (1.7)	1.6 (1.8)	~2.0	2.5 (2.8)	**2.5** (3.1)	2.3
$^3J_{C2,H4}$	0.9 (1.1)	0.9 (0.9)	~0.9	0.6 (0.9)	**0.6** (0.7)	0.0
$^3J_{C3,H1}$	**5.2** (4.7)	**5.0** (4.9)	5.2	1.1 (1.5)	1.1 (1.5)	1.1
$^3J_{C3,H5}$	**2.2** (2.1)	2.3 (2.0)	~2.3	2.5 (2.5)	2.7 (2.3)	2.2
$^3J_{C4,H2}$	**1.0** (1.5)	0.9 (1.3)	0.9	0.9 (1.2)	0.9 (1.1)	1.1
$^3J_{C5,H1}$	6.9 (7.6)	6.6 (6.9)	6.5	0.9 (1.1)	**1.0** (1.3)	1.0
$^3J_{C5,H3}$	1.1 (1.3)	1.0 (1.0)	0.9	1.0 (1.2)	**0.8** (1.0)	1.1
$^3J_{C6,H4}$	3.0 (3.6)	2.8 (3.2)	3.6	2.9 (3.5)	**2.6** (3.0)	3.5

[a]At 30 °C in ^2H_2O; ± 0.1 Hz. Coupling constants in bold were obtained by spectral simulation using MacNuts software.[17] [b]Calculated J_{CH} (in parentheses) were obtained by averaging the full data set of calculated couplings (12 values of $\omega \times 3$ fixed values of θ = 36 couplings) (see Calculational Methods). Couplings in **4** and **5** were taken from previous work.[16,18]

Table 6. Experimental $^1J_{CC}$[a] in 2 and 3 at pD 2.0 and 7.0, and Calculated $^1J_{CC}$[b] in 2_c^p, 2_c^i, 3_c^p and 3_c^i

	2			3		
$^1J_{CC}$ (Hz)	pD 2.0	pD 7.0	Me α-Glc*p* **4**	pD 2.0	pD 7.0	Me β-Glc*p* **5**
$^1J_{C1,C2}$	46.5 (46.9)	46.5 (47.2)	46.6	46.9 (47.9)	46.8 (48.1)	46.8
$^1J_{C2,C3}$	38.4 (40.7)	38.5 (40.6)	38.3	39.2 (41.2)	39.1 (41.2)	39.0
$^1J_{C3,C4}$	38.8 (43.3)	38.9 (42.4)	38.6	39.5 (43.9)	39.5 (43.2)	39.3
$^1J_{C4,C5}$	37.7 (40.3)	38.8 (41.9)	40.4	38.3 (41.1)	38.6 (42.6)	41.0
$^1J_{C5,C6}$	64.1 (65.4)	59.1 (61.3)	43.3	64.2 (65.4)	59.0 (61.5)	43.3

[a]At 30 °C in ^2H_2O; ± 0 0.1 Hz. [b]Calculated $^1J_{CC}$ (in parentheses) were obtained by averaging the full data set of calculated couplings (12 values of $\omega \times 3$ fixed values of θ = 36 couplings) (see Calculational Methods). Couplings in **4** and **5** were taken from previous work.[12,24]

and/or the C3−C4−C5−H5 torsion angle is smaller than the 60° angle found in the idealized $^4C_1$ ring conformation.

Unlike the behavior of calculated $^2J_{CH}$, calculated $^3J_{CH}$ are generally in good agreement with experimental $^3J_{CH}$, even for the "anomalous" $^3J_{C3,H5}$. The improved agreement is partly caused by the reduced sensitivity of $^3J_{CH}$ to exocyclic C−O bond conformation compared to $^2J_{CH}$ (i.e., C−O bond torsions exert a greater effect on $^2J_{CH}$ than on $^3J_{CH}$).

E. $^{13}C-^{13}C$ Spin-Coupling Constants. *1. One-Bond Couplings.* $^1J_{C1,C2}$, $^1J_{C2,C3}$ and $^1J_{C3,C4}$ in **2** and **3** are unaffected by COOH ionization state and are very similar to corresponding $^1J_{CC}$ in **4** and **5** (Table 6). $^1J_{C2,C3}$ and $^1J_{C3,C4}$ are slightly larger in **3** than in **2**, in both the protonated and ionized forms; this behavior mimics that observed in **4** and **5**.

$^1J_{C4,C5}$ and $^1J_{C5,C6}$ in **2** and **3** differ from corresponding values in **4** and **5**, with the former ~2 Hz smaller and the latter ~18 Hz larger in the uronides (Table 6). $^1J_{C4,C5}$ increases by ~0.7 Hz and $^1J_{C5,C6}$ decreases by ~5 Hz upon COOH ionization. $^1J_{C4,C5}$ is slightly affected by anomeric configuration in the COOH forms but not in the COO^- forms. $^1J_{C5,C6}$ shows no dependence on anomeric configuration, in concert with the behavior of $^1J_{C5,C6}$ in **4**/**5**.

Calculated $^1J_{C5,C6}$ is smaller in 2_c^i and 3_c^i than in 2_c^p and 3_c^p by ~5 Hz, in agreement with experiment. This behavior presumably reflects the effect of ionization on $r_{C5,C6}$, which increases by 0.02 − 0.03 Å upon COOH ionization (Figure S4, Supporting Information). Similar behavior was observed in DFT studies of *N*-acetyl-neuraminic acid (NANA).[25] In NANA, $^1J_{C1,C2}$ decreases upon COOH ionization by ~5 Hz; an hyperconjugative model was proposed to explain the observed lengthening of the C1−C2 bond, and reduced $^1J_{C1,C2}$, upon COOH ionization.

Calculated $^1J_{CC}$ display the general trends observed experimentally; $^1J_{C1,C2}$ values are intermediate in magnitude between $^1J_{C2,C3}$, $^1J_{C3,C4}$ and $^1J_{C4,C5}$ (~38 Hz) and $^1J_{C5,C6}$ (~63 Hz) (Table 6). The level of agreement with experiment varies from site to site, with disparities partly attributed to insufficient modeling of the exocyclic C−O torsions (C−O bond torsions in HO−C−C-OH fragments significantly affect the associated $^1J_{CC}$[26]).

$^1J_{CC}$ values for C−C fragments near the exocyclic COOH group depend on ω, but the magnitude of the effect does not correlate directly with degree of proximity. $^1J_{C5,C6}$ in 2_c^i and 3_c^i changes by 1−2 Hz upon 360° rotation of ω (Figure 8),

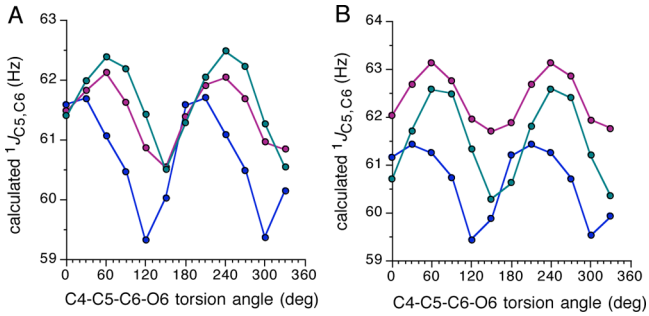

Figure 8. Effect of ω on calculated $^1J_{C5,C6}$ in 2_c^i (A) and 3_c^i (B). Green, θ = 60°; red, θ = 180°; blue, θ = −60°.

whereas $^1J_{C4,C5}$ changes by 4−6 Hz (Figure 9). Calculated $^1J_{C4,C5}$ values are smallest in geometries having the C4−C5 bond orthogonal to the carboxylate plane, and largest when the torsion angle between the carboxylate oxygens and C4 is 0° and 180° (carboxylate plane parallel to the C4−C5 bond). These effects correlate approximately with $r_{C4,C5}$ (Figure S5, Supporting Information), with shorter bonds (greater *s*-character) giving larger $^1J_{C4,C5}$.

dx.doi.org/10.1021/jo3011182 | J. Org. Chem. 2012, 77, 9521−9534

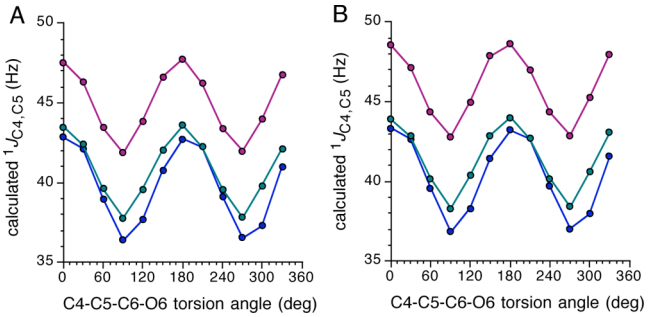

Figure 9. Effect of ω on calculated $^1J_{C4,C5}$ in $\mathbf{2}_c^i$ (A) and $\mathbf{3}_c^i$ (B). Green, $\theta = 60°$; red, $\theta = 180°$; blue, $\theta = -60°$.

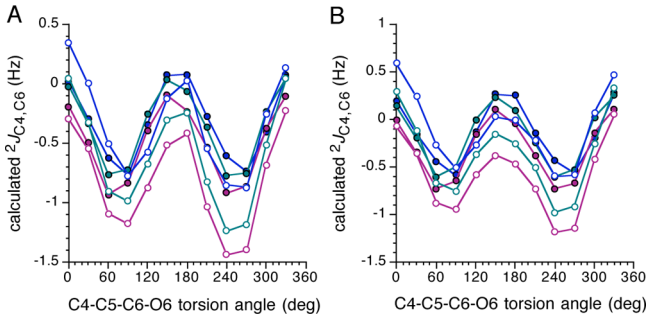

Figure 10. Effect of ω on calculated $^2J_{C4,C6}$ in $\mathbf{2}_c$ (A) and $\mathbf{3}_c$ (B). Open symbols, $\mathbf{2}_c^p$ and $\mathbf{3}_c^p$. Filled symbols, $\mathbf{2}_c^i$ and $\mathbf{3}_c^i$. Green, $\theta = 60°$; red, $\theta = 180°$; blue, $\theta = -60°$.

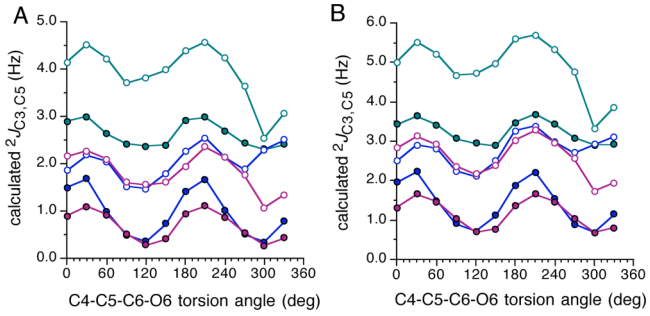

Figure 11. Effect of ω on calculated $^2J_{C3,C5}$ in $\mathbf{2}_c$ (A) and $\mathbf{3}_c$ (B). Open symbols, $\mathbf{2}_c^p$ and $\mathbf{3}_c^p$. Filled symbols, $\mathbf{2}_c^i$ and $\mathbf{3}_c^i$. Green, $\theta = 60°$; red, $\theta = 180°$; blue, $\theta = -60°$.

2. Two-bond Couplings. $^2J_{C1,C3}$, $^2J_{C2,C4}$, and $^2J_{C1,C5}$ in **2** and **3** are unaffected by COOH ionization, and their magnitudes and signs[27] are identical to corresponding $^2J_{CC}$ in **4** and **5** (Table 7). All three $^2J_{CC}$ depend on anomeric configuration, with $^2J_{C1,C3}$ showing the largest change (~4.5 Hz larger in **3**), followed by $^2J_{C1,C5}$ (more negative in **2** by ~2 Hz), and $^2J_{C2,C4}$ (~0.4 Hz more positive in **2**). These trends mimic those found in **4** and **5**.[24,28]

$^2J_{C3,C5}$ and $^2J_{C4,C6}$ depend on the ionization state of the COOH group (Table 7). The effect is greater for the more remote $^2J_{C3,C5}$. $^2J_{C3,C5}$ is positive in sign and ~1 Hz larger in $\mathbf{2}^p$ and $\mathbf{3}^p$ than in $\mathbf{2}^i$ and $\mathbf{3}^i$. $^2J_{C4,C6}$ is negative in sign in **2** and **3** (based on DFT results), with COOH ionization causing a small (~0.3 Hz) shift to less negative values. Both $^2J_{CC}$ differ from corresponding values in **4** and **5**, although the differences are small (<1.3 Hz).

Calculated $^2J_{CC}$ show moderate agreement with experiment, with differences of <1 Hz observed (Table 7). The computations predict the correct dependence of $^2J_{C3,C5}$ and $^2J_{C4,C6}$ on ionization state and on anomeric configuration. $^2J_{C4,C6}$ in $\mathbf{2}_c$ and $\mathbf{3}_c$ shows a small dependence on ω in both the protonated and ionized forms, with the smallest (most negative) couplings predicted for ω of ~60° and ~240° (carboxyl plane parallel to the C5–H5 bond) (Figure 10). $^2J_{C3,C5}$ shows a modest dependence on ω (Figure 11), and unlike $^2J_{C4,C6}$, θ significantly affects its magnitude, with an ~1.5 Hz increase observed for $\theta = 60°$ vs $\theta = -60°$ and 180°, that is, when O4H is *anti* to H4 and the lone-pair orbitals on O4 are *anti* to the C3–C4 and C4–C5 bonds. This effect is similar to that observed for $^2J_{C1,C3}$, where rotation of the central C2–O2 bond affects the observed coupling significantly.[29] However, apart from the effect of θ on $^2J_{C3,C5}$, ω exerts only a small effect (1 Hz or less) on calculated $^2J_{C3,C5}$ (Figure 11).

3. Three-bond Couplings. Three-bond $^{13}C-^{13}C$ spin-couplings depend largely on the dihedral angle between the coupled terminal carbons and are normally positive in sign.[12,24]

In **2** and **3**, two single-pathway $^3J_{CC}$ exist, namely, $^3J_{C1,C6}$ and $^3J_{C3,C6}$. Both couplings depend on anomeric configuration, with ~0.8 Hz larger couplings observed in **3** in both the protonated and ionized forms (Table 8); these trends mimic those found in **4** and **5**. $^3J_{C1,C6}$ and $^3J_{C3,C6}$ depend on COOH ionization state, with ~0.5 Hz smaller couplings observed in the ionized form. $^3J_{C1,C6}$ and $^3J_{C3,C6}$ are ~1 Hz larger in **2** and **3** relative to corresponding values in **4** and **5**.

$^{13}C-^{13}C$ Spin-couplings between C1 and C4, and between C2 and C5, involve dual pathways.[24] As found in **4** and **5**, $^{3+3}J_{C1,C4}$ and $^{3+3}J_{C2,C5}$ are very small or zero in **2** and **3**; the structural dependencies of these couplings have been discussed previously.[24]

Calculated $^3J_{CC}$ reproduce the experimental data well, with differences typically <0.4 Hz (Table 8). $^3J_{C1,C6}$ is largely unaffected by ω in $\mathbf{2}_c$ and $\mathbf{3}_c$, especially in the ionized forms (data not shown). In contrast, θ does influence $^3J_{C3,C6}$, especially in the ionized forms (Figure 12). Whereas the curves for $\theta = 60°$ and 180° are relatively flat, that for $\theta = -60°$

Table 7. Experimental $^2J_{CC}$[a] in 2 and 3 at pD 2.0 and 7.0, and Calculated $^2J_{CC}$[b] in $\mathbf{2}_c^p$, $\mathbf{2}_c^i$, $\mathbf{3}_c^p$ and $\mathbf{3}_c^i$

	2			**3**		
$^2J_{CC}$ (Hz)	pD 2.0	pD 7.0	Me α-Glcp **4**	pD 2.0	pD 7.0	Me β-Glcp **5**
$^2J_{C1,C3}$	0 (−0.6)	0 (−0.6)	0	4.7 (4.3)	4.6 (4.2)	4.5
$^2J_{C1,C5}$	1.8 (−1.9)	2.0 (−2.6)	2.0	0.0 (0.5)	0.0 (−1.2)	0
$^2J_{C2,C4}$	3.1 (2.8)	3.1 (2.5)	3.1	2.7 (2.4)	2.7 (2.1)	2.6
$^2J_{C3,C5}$	1.9 (2.6)	0.9(1.4)	1.7	2.8 (3.4)	1.8 (1.9)	~2.3
$^2J_{C4,C6}$	1.3 (−0.6)	1.1 (−0.4)	0	1.2 (−0.3)	0.9 (−0.2)	0

[a]At 30 °C in ^2H_2O; ± 0.1 Hz. [b]Calculated $^2J_{CC}$ (in parentheses) were obtained by averaging the full data set of calculated couplings (12 values of $\omega \times 3$ fixed values of $\theta = 36$ couplings) (see Calculational Methods). Couplings in **4** and **5** were taken from previous work.[12,24]

dx.doi.org/10.1021/jo3011182 | J. Org. Chem. 2012, 77, 9521–9534

Table 8. Experimental $^{3}J_{CC}$ and $^{3+3}J_{CC}$[a] in 2 and 3 at pD 2.0 and 7.0, and Calculated $^{3}J_{CC}$ and $^{3+3}J_{CC}$[b] in 2_c^p, 2_c^i, 3_c^p and 3_c^i

	2			3		
$^{3}J_{CC}$ (Hz)	pD 2.0	pD 7.0	Me α-Glcp 4	pD 2.0	pD 7.0	Me β-Glcp 5
$^{3}J_{C1,C6}$	4.2 (4.7)	3.9 (4.0)	3.3	5.5 (6.0)	4.9 (5.1)	4.2
$^{3}J_{C3,C6}$	4.9 (5.2)	4.5 (4.2)	3.8	5.5 (5.7)	5.0 (4.6)	4.2
$^{3+3}J_{C1,C4}$	0 (0)	0 (0.1)	0	0 (−0.3)	0 (−0.2)	0
$^{3+3}J_{C2,C5}$	0 (0.6)	0 (0.6)	0	0 (−0.2)	0 (−0.2)	0

[a]At 30 °C in $^{2}H_2O$; ± 0.1 Hz. [b]Calculated J_{CC} (in parentheses) were obtained by averaging the full data set of calculated couplings (12 values of ω × 3 fixed values of θ = 36 couplings) (see Calculational Methods). Couplings in 4 and 5 were taken from previous work.[12,24]

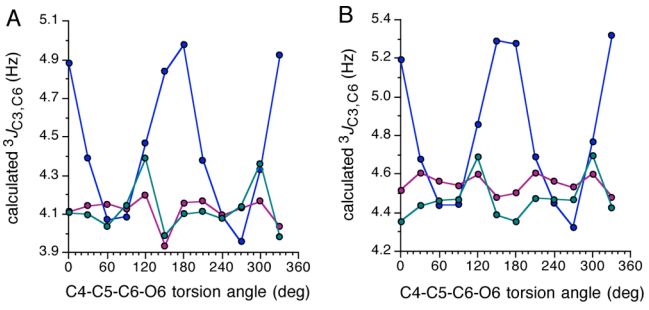

Figure 12. Effect of ω on calculated $^{3}J_{C3,C6}$ in 2_c^i (A) and 3_c^i (B). Green, θ = 60°; red, θ = 180°; blue, θ = −60°.

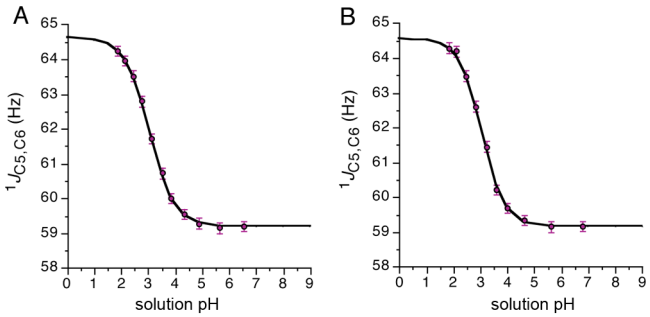

Figure 13. pH-Induced changes in $^{1}J_{C5,C6}$ in 2 (A) and 3 (B). Data points are the experimental data; black line shows the experimental data fit to eq 1, from which pK_a values were determined (see text). Error bars: ± 0.15 Hz.

shows a greater dependence on ω; in this case, H-bonding between O4H (donor) and the carboxylate (acceptor) at ω = 0° and 180° enhances the coupling.

F. pK_a Values in 2 and 3. Carboxyl pK_a values in 2 and 3 were determined by measuring the pH dependencies of C6 chemical shifts. To minimize ^{2}H isotope effects, NMR spectra were obtained in 95:5 (v/v) $^{1}H_2O/^{2}H_2O$ solvent. Titration data (Figure S6, Supporting Information) were fit to a modified Henderson−Hasselbach equation (eq 1)[30]

$$\delta(\mathrm{pH}) = \frac{\delta_{base} + [\delta_{acid}(10^{(pK_a - pH)n})]}{1 + 10^{(pK_a - pH)n}} \quad (1)$$

where δ(pH) is the observed chemical shift, δ_{acid} and δ_{base} are the limiting chemical shifts, respectively, and n is the Hill coefficient that can assume a value of 1.0 or greater. Parameters δ_{acid}, δ_{base}, pK_a and n were optimized simultaneously using the Solver Routine in Microsoft Excel.

pK_a Values determined from the data given in Figure S6 (Supporting Information) were: 2, 3.0 ± 0.1; 3, 3.0 ± 0.1. These values compare favorably with the pK_a of 2.9 determined by direct titration with NaOH (Figure S7, Supporting Information) and are similar to that reported for D-riburonic acid (pK_a 2.9).[15] Anomeric configuration appears to exert little or no effect on the acidity of the exocyclic COOH substituent.

pK_a Values were also obtained from studies of the effect of pH on select J-couplings. $^{1}J_{C5,C6}$ is particularly suited to this treatment because of its relatively large dependence on solution pH (Figure 13); these data gave a pK_a of 3.0 for 2 and 3.1 for 3. Some J_{CH} and ^{1}H chemical shifts also yielded pK_a values; for example, the use of $^{2}J_{C6,H5}$ and δ_{H5} in 2 is illustrated in Figure S8 (Supporting Information). Longer-range J_{CC} such as $^{2}J_{C4,C6}$, $^{3}J_{C1,C6}$ and $^{3}J_{C3,C6}$ were also suitable for pK_a determinations, although their pH dependencies are modest compared to that of $^{1}J_{C5,C6}$, leading to less accurate determinations (Figure S9, Supporting Information).

G. Structural Insights from X-ray Crystal Structures. The observed differences in J-couplings in methyl aldohexopyranosides 4 and 5 and their corresponding uronides 2 and 3 presumably reflect their different molecular structures. Insight into these structural differences was sought by comparing the X-ray structures of β-D-glucopyranose 8[31] and sodium β-D-glucopyranuronate 9[32] (Table S3, Supporting Information). Corresponding bond lengths in the two structures are very similar except for $r_{C5,C6}$, $r_{C4,C5}$, and $r_{C4,O4}$. The C5−C6 bond length is 0.019 Å longer in the uronic acid. Thus, factors in addition to bond length must determine $^{1}J_{C5,C6}$, since this J-coupling is much larger in 2/3 than in 4/5 (Table 6). If bond length were the only determinant, then $^{1}J_{C5,C6}$ should be smaller in the uronic acid (i.e., longer C5−C6 bond → less s-character → smaller coupling). The difference in hybridization (and thus geometry) at C6 in 2/3 and 4/5 probably accounts for the observed behavior, that is, the C5−C6 bond in 2/3 has intrinsically greater s-character than that in 4/5 by virtue of its different hybridization. J-Coupling predictions based on bond length in these different systems is therefore unreliable. The C4−C5 bond length is ∼0.15 Å longer in 9 than in 8. In contrast, $r_{C4,O4}$ is shorter in 9 by 0.016 Å. Endocyclic bond angles are similar in 8 and 9 except for the C1−C2−C3 bond angle, which is ∼4° smaller in the latter. The exocyclic C4−C5−C6 bond angle is ∼6° smaller in 9 than in 8. Some of these changes may be induced partly by differences in ring conformation. Cremer-Pople parameters for the two structures are: for 8, Q = 0.5802, θ = 7.89, ϕ = 318.1707, q_2 = 0.0796, q_3 = 0.5747; for 9, Q = 0.5941, θ = 9.08, ϕ = 37.2234, q_2 = 0.0938, q_3 = 0.5867. While the degree of ring distortion is similar in both structures (similar θ), the directions of distortion (ϕ) differ, with 9 skewed slightly toward $^{C3}TB_{C1}$ and 8 toward $^{O5}TB_{C2}$. While solid-state conformation may differ from that in solution, it is likely that many of the changes observed in J-couplings between 2/3 and 4/5 are mediated by differences in r_{CC} and r_{CH}. The pyranosides and uronates have similar overall structures, but they are not identical, especially in the region close to the C6 exocyclic substituent.

dx.doi.org/10.1021/jo3011182 | J. Org. Chem. 2012, 77, 9521−9534

H. ^{1}H and ^{13}C Chemical Shifts in Methyl α-D-Glucopyranosiduronic 2 and Methyl α-D-Glucopyranoside 4. A solution containing a 1:1 mixture of methyl α-D-[6-^{13}C]glucopyranuronic acid **2** and methyl α-D-[6-^{13}C]glucopyranoside **4** in ^2H_2O solvent was prepared to examine the effect of C6 structure on ^{1}H and ^{13}C chemical shifts at two solution pHs (Table 9). The observed differences in ^{13}C chemical shifts do not scale directly with proximity to the site of substitution. For example, differences of −1.0 ppm (pH 2.0) and +0.4 ppm (pH 7.2) are observed for δ_{C5}, whereas differences of +1.8 (pH 2.0) and +2.4 ppm (pH 7.2) are observed for δ_{C4}. In contrast, δ_{H5} changes more than δ_{H4} at pH 2.0 and 7.2. The effects on δ_{C4} and δ_{H4} are probably through-space; presumably the local magnetic field anisotropy of the carboxyl group induces a downfield shift in the C4 signal of the uronic acid. The magnitude of the latter effect is likely determined by the conformational properties of the C5−C6 bond in solution (i.e., the orientation of the carboxyl plane with respect to C4 and H4).

Table 9. ^{13}C and ^{1}H Chemical Shift Differences Between Methyl α-D-[6-^{13}C]Glucopyranosiduronic Acid 2 and Methyl α-D-[6 ^{13}C]Glucopyranoside 4

CS difference[a]	C1	C2	C3	C4	C5	CH_3
pH 2.0	0.313	−0.421	−0.455	1.837	−0.988	0.515
pH 7.2	0.062	−0.167	−0.213	2.431	0.379	0.169
CS difference	H2	H3	H4		H5	CH_3
pH 2.0	0.060	0.039	0.171		∼0.50	0.026
pH 7.2	0.040	0.012	0.095		∼0.26	0.006

[a]Defined as $\delta_{Me\alpha GlcUA} - \delta_{Me\alpha Glc}$; in ppm, 22 °C, ^2H_2O solvent.

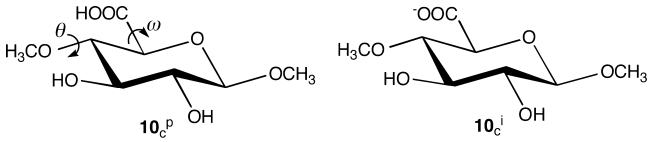

I. Implications For Studies of Glycosidic Linkage Conformation. Theoretical studies of model compounds $\mathbf{10}_c^P$ and $\mathbf{10}_c^i$ were undertaken to evaluate the application of *J*-couplings to investigate *O*-glycosidic linkage conformation involving glucuronic acid residues. In these studies, the uronic acid serves as an acceptor in a β-(1→4) linkage like that shown in **1**. The aim was to identify ^{13}C−^{1}H and ^{13}C−^{13}C spin-couplings that may report on one of the linkage torsions, namely, *psi* (ψ) (Scheme 1). The expectation that the five *J*-couplings in Scheme 1 ($^1J_{C3,C4}$, $^1J_{C4,C5}$, $^2J_{C3,C5}$, $^2J_{C3,H4}$ and $^2J_{C5,H4}$) might depend on ψ is based on prior findings that are summarized as follows: (a) $^1J_{CC}$ values in OH−C−C−OH fragments are sensitive to rotations of the central C−C bond and both C−O bonds, with the latter rotations inducing greater change;[26] $^2J_{CCC}$ values in OH−C−C(OH)−C−OH fragments are less sensitive to rotations of the C−O bonds on the terminal carbons than to rotation of the C−O bond on the central carbon;[29] $^2J_{CCH}$ values in OH−C−C(OH)(H) fragments (coupled nuclei underlined) are more sensitive to rotation of the C−O bond involving the carbon bearing the coupled proton than to rotation of the C−O bond on the coupled carbon.[23] Prior work has shown that the ψ torsion angle can be studied from the donor side of the linkage by measuring $^2J_{C1',C4}$, $^3J_{C2',C4}$ and $^3J_{C4,H1'}$ (Scheme 1);[12−14] the present work aimed to potentially expand this ensemble to include spin-couplings on the acceptor side.

Scheme 1. *J*-Couplings Potentially Sensitive to ψ

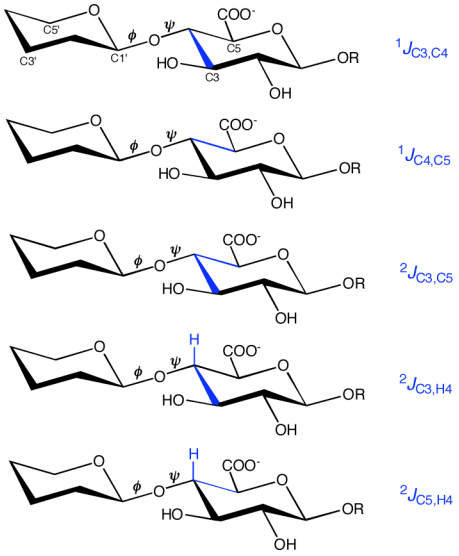

The presence of an *O*-methyl group at C4 of $\mathbf{10}_c$ allowed an assessment of its influence on conformational energies. A discussion of these findings can be found in the Supporting Information. Herein we focus on the DFT-derived *J*-couplings and their potential as probes of ψ.

The influence of ω and θ on $^1J_{C3,C4}$ and $^1J_{C4,C5}$ in $\mathbf{10}_c^i$ is shown in Figure 14 (data for $\mathbf{10}_c^P$ are shown in Figure S10, Supporting Information). For $^1J_{C3,C4}$, the largest coupling is observed for θ = −60° (∼46.5 Hz); for θ = 60° and 180°, $^1J_{C3,C4}$ is reduced to 42−43 Hz (Figure 14A). When θ = 60° and 180°, a lone-pair orbital on O4 is oriented *anti* to the C3−C4 bond, resulting in C−C bond elongation, which presumably contributes to the reduction in $^1J_{C3,C4}$. In a similar vein, $^1J_{C4,C5}$ is largest in $\mathbf{10}_c^i$ when θ = 180° compared to θ = 60° and −60° (Figure 14B) (data for $\mathbf{10}_c^P$ are shown in Figure S10, see Supporting Information). In the latter geometries, a lone-pair on O4 is *anti* to the C4−C5 bond. The effect of ω on these $^1J_{CC}$ differs; $^1J_{C3,C4}$ is much less sensitive to C5−C6 bond rotation than is $^1J_{C4,C5}$; since the latter coupling involves one of the carbons (C5) of the rotating ω bond, presumably the effect is more directly transmitted to $^1J_{C4,C5}$. Both $^1J_{CC}$ display a calculated dynamic range of ∼4 Hz with respect to rotation about ψ; this range may be greater if the full rotation about ψ were inspected.

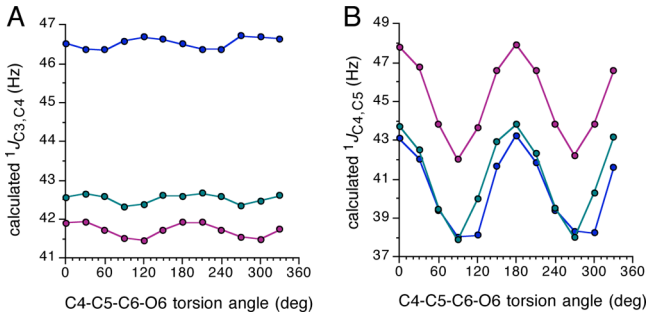

Figure 14. Effect of ω on $^1J_{C3,C4}$ (A) and $^1J_{C4,C5}$ (B) in $\mathbf{10}_c^i$. Data for θ of 60°, −60° and 180° are shown in green, blue and red, respectively.

Like $^1J_{C3,C4}$ and $^1J_{C4,C5}$, $^2J_{C3,C5}$ exhibits a dependence on θ in $\mathbf{10}_c^i$ (Figure 15A) (data for $\mathbf{10}_c^P$ are shown in Figure S11, Supporting Information). Calculated couplings are positive in

dx.doi.org/10.1021/jo3011182 | J. Org. Chem. 2012, 77, 9521−9534

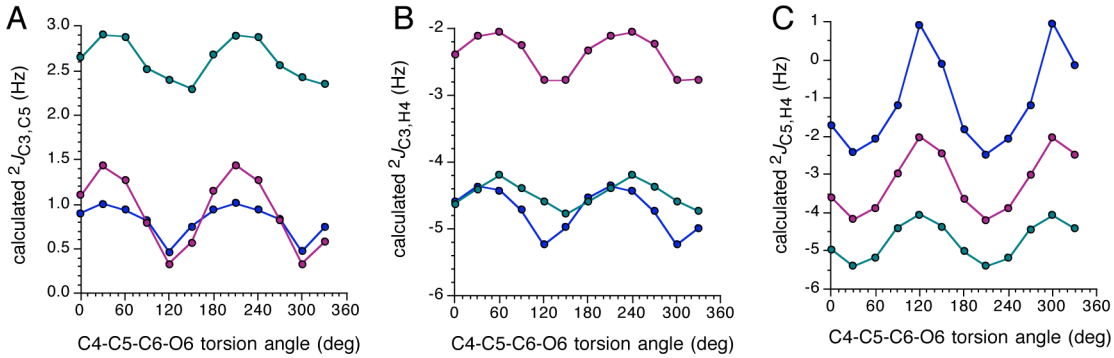

Figure 15. Effect of ω on $^2J_{C3,C5}$ (A), $^2J_{C3,H4}$ (B) and $^2J_{C5,H4}$ (C) in $\mathbf{10}_c^i$. Data for θ of 60°, −60° and 180° are shown in green, blue and red, respectively.

sign in all cases examined, and are maximal when θ = 60° (2.5−3.0 Hz), with smaller couplings in the 0.5−1.5 Hz range when θ = −60° and 180°. $^2J_{C3,C5}$ exhibits a smaller (absolute) dependence on ω (~1 Hz) than does $^1J_{C4,C5}$ (~6 Hz; Figure 14B). When θ = 60°, the two lone-pair orbitals on O4 are *anti* to the C3−C4 and C4−C5 bonds; this C−O rotamer has been shown to enhance $^2J_{CCC}$ in simpler model systems.[29] When one of these *anti* lone-pair orbitals is replaced by the O4−H bond (at θ = −60° or 180°), a smaller (less positive) coupling is produced. Based only on the three staggered geometries about θ, a dynamic range of 1.5−2.0 Hz is predicted for $^2J_{C3,C5}$ with respect to rotation about ψ.

The dependencies of $^2J_{C3,H4}$ and $^2J_{C5,H4}$ on both ω and θ in $\mathbf{10}_c^i$ are shown in Figure 15B,C (data for $\mathbf{10}_c^P$ are shown in Figure S12, Supporting Information). Calculated values of $^2J_{C3,H4}$ are negative and fall into two groups, those near −2 Hz, and those near −5 Hz. The least negative (most positive) coupling corresponded to θ = 180°. In the latter structure, the two lone-pair orbitals on O4 are *anti* to the C3−C4 and C4−H4 bonds; presumably the expected C−C and C−H bond elongations shift the coupling to more positive values. The effect of ω on $^2J_{C3,H4}$ is small (<1 Hz), and the overall dynamic range with regard to ψ, deduced from inspection of only the three staggered values of θ, is ~2.5 Hz. Calculated $^2J_{C5,H4}$ are also largely negative in sign, with the least negative associated with θ = −60° and the most negative associated with θ = 60°. As found for $^2J_{C3,H4}$, in the structure having the least negative coupling (θ = −60°), the two lone-pair orbitals on O4 are *anti* to the C4−C5 and C4−H4 bonds. In this case, however, the remaining two θ rotamers are not equivalent, suggesting that contraction of the C4−C5 bond (θ = 180°) exerts a smaller effect on $^2J_{C5,H4}$ than does contraction of the C4−H4 bond (θ = 60°). $^2J_{C5,H4}$ is more sensitive to ω than $^2J_{C3,H4}$, presumably for the same reasons that $^1J_{C5,C4}$ is more sensitive to ω than $^1J_{C3,C4}$.

CONCLUSIONS

^{1}H and ^{13}C NMR analyses of singly-^{13}C-labeled isotopomers of methyl α- and methyl β-D-glucopyranuronides have yielded a complete set of ^{13}C−^{1}H and ^{13}C−^{13}C spin-couplings at pD 2 and pD 7. In conjunction with J_{HH}, these *J*-couplings pertain to an aldohexopyranosiduronic acid that highly prefers the $^4C_1$ ring conformation in both anomers in solution regardless of COOH ionization state. Thus, changes in experimental *J*-couplings in **2** and **3** induced by the ionization of the exocyclic COOH group do not arise from changes in ring conformation to any appreciable extent, but rather arise from intrinsic changes in electronic structure and/or changes in exocyclic conformations (e.g., C−O and C−C bond rotations). This "rigid" system provides a useful baseline for the analysis of related *J*-couplings in uronic acids possessing greater conformational flexibility, such as L-idohexopyranuronic acid **11**. In **11**, a change in COOH ionization state may affect ring conformational preference, which would be reflected in changes in NMR *J*-couplings. The latter changes derive from three sources: (1) intrinsic effects on electronic structure that are independent of ring conformation; (2) conformational change in the ring; and (3) conformational change in exocyclic substituents. Contributions from the intrinsic effects, and to a lesser extent exocyclic conformational factors, were the focus of the present work where they could be decoupled from the ring conformation factor. It is noteworthy that the solution conformation of the flexible aldopenturonic acid **7** depends on COOH ionization state; percentages of α- and β-furanoses in aqueous solutions depend on solution pH, an effect apparently caused by differences in furanose ring phase angles and/or amplitudes in the protonated and ionized states.[15] Prior work has shown that divalent metal complexation with **3** does not affect ring conformation appreciably, whereas with structures like **11** (α-anomer) significant ring conformational change occurs, as indicated from changes in ^{1}H and ^{13}C chemical shifts, and ^{1}H−^{1}H spin couplings.[33] These effects might be investigated in greater detail with the use of the *J*-coupling ensembles discussed in this report.

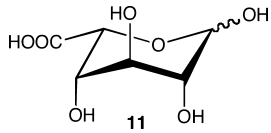

11

Structural comparisons were made herein between an uronic acid and its corresponding uronate to quantify the effects of COOH ionization, and between an uronic acid/uronate and the corresponding methyl aldopyranoside to quantify the effect of substituting an exocyclic COOH/COO$^-$ group for a CH_2OH group at C5. Key findings are summarized in the following paragraphs.

Experimental J_{HH}, J_{CH} and J_{CC} in **2** and **3** are essentially unaffected by the ionization state of the COOH group, with most changes ≤0.8 Hz. *J*-Couplings that change by ≥0.8 Hz include $^1J_{C1,H1}$ ($\Delta \approx 0.8$ Hz), $^1J_{C4,H4}$ ($\Delta \approx 0.8$ Hz), $^1J_{C5,H5}$ ($\Delta \approx 3$ Hz), $^1J_{C5,C6}$ ($\Delta \approx 5$ Hz), and $^2J_{C3,C5}$ ($\Delta \approx 1$ Hz). Spin-couplings showing the greatest dependence are close to the site of ionization from a bonding viewpoint, although the magnitude of the effect does not track inversely with the number of intervening bonds; for example, the effect of COOH

dx.doi.org/10.1021/jo3011182 | J. Org. Chem. 2012, 77, 9521−9534

ionization on $^{2}J_{C3,C5}$ is greater than that on $^{2}J_{C4,C6}$. Several *J*-couplings, and ^{1}H and ^{13}C chemical shifts, sensitive to COOH ionization state were titrated to give pK_a values of ∼3.0 for **2** and **3**. While often less sensitive than chemical shifts, *J*-couplings may be attractive as *in situ* pH indicators, since the local (intermolecular) environment probably influences them less than chemical shifts, eliminating the need for an internal reference.[34] For example, use of [5,6-$^{13}C_2$]**2** or **3** as a pH probe could simplify the measurement of $^{1}J_{C5,C6}$ in complex mixtures, from which local pH could be determined. In principle, a set of *J*-couplings could be developed that would allow measurement of solution pH over a wide pH range.[35]

pK_a Values of **2** and **3** (and **7**[12]) are smaller than those of simple carboxylic acids such as formic acid (pK_a 3.77), acetic acid (pK_a 4.76) and lactic acid (pK_a 3.86). Proximity of the anomeric center to the ionization site, a consequence of ring closure, increases the acidity of the COOH group, possibly by providing an electron sink for, and stabilization of, the ionized state. Alternatively, the enhanced acidity could be caused by destabilization of the protonated state. Thus, pK_a values for open-chain (acyclic) aldehyde and hydrate forms of aldohexopyranuronic acids should be larger (less acidic) than those of cyclic forms. Recent work has shown that cyclic forms of NANA **6** are less acidic (pK_a ∼2.5) than the acyclic *keto* form (pK_a ∼2.0) but more acidic than the acyclic *enol* form (pK_a ∼5.5).[36] Presumably the greater acidity of the acyclic *keto* form of **6** is promoted by the carbonyl group at C2, which serves as a more potent electron sink than the hemiketal functionality in the cyclic forms.

Comparisons between NMR parameters in the **2**/**3** with those in corresponding methyl aldopyranosides **4**/**5** reveal the effects of substituting an exocyclic hydroxymethyl group at C5 with a carboxylate. The four J_{HH} in **2**/**3** are very similar to corresponding couplings in **4**/**5**, with observed changes <0.3 Hz, suggesting similar ring conformations. All $^{1}J_{CH}$ except $^{1}J_{C4,H4}$ and $^{1}J_{C5,H5}$ are insensitive to the change in C5 substitution; for $^{1}J_{C4,H4}$ and $^{1}J_{C5,H5}$, differences of 1−3 Hz and 3−6 Hz were observed, respectively, with larger couplings found in **2**/**3**. Of the nine $^{2}J_{CCH}$ investigated, seven are insensitive to the change in C5 substitution; $^{2}J_{C4,H5}$ is ∼1 Hz more negative, and $^{2}J_{C5,H4}$ is ∼0.6 Hz more positive, in **2**/**3** compared to **4**/**5**. The most significant change was observed in $^{2}J_{C6,H5}$, which is ∼2.5 Hz more negative in **2**/**3** than in **4**/**5**. For $^{3}J_{CH}$, only $^{3}J_{C6,H4}$ is affected by the C5 substitution change, being ∼1 Hz smaller in **2**/**3** than in **4**/**5**. Within $^{1}J_{CC}$, only $^{1}J_{C4,C5}$ and $^{1}J_{C5,C6}$ are affected, being ∼2 Hz smaller and ∼18 Hz larger, respectively, in **2**/**3** than in **4**/**5**. Of the five $^{2}J_{CC}$ measured, three are insensitive to a change in C5 substitution; changes in $^{2}J_{C3,C5}$ and $^{2}J_{C4,C6}$ are small (<1.3 Hz) and depend on the COOH ionization state. Of the four $^{3}J_{CC}$ investigated, two are affected by a change in C5 substitution; $^{3}J_{C1,C6}$ and $^{3}J_{C3,C6}$ are larger in **2**/**3** by ∼1 Hz. These results are summarized in Table 10.

Solvated DFT calculations of *J*-couplings predict trends consistent with the experimental data and yield *J*-couplings in reasonable agreement with experiment. To support this claim, data in Table 11 compare five experimental *J*-couplings most affected by COOH ionization state ($^{1}J_{C1,H1}$, $^{1}J_{C4,H4}$, $^{1}J_{C5,H5}$, $^{1}J_{C5,C6}$, and $^{2}J_{C3,C5}$) with corresponding DFT-calculated values. Calculated one-bond $^{13}C-^{1}H$ and $^{13}C-^{13}C$ *J*-couplings are consistently larger than experimental values by ∼2.2%, and the errors appear about the same for *J*-couplings calculated in the protonated (neutral) and ionized structures. Calculated geminal $^{13}C-^{13}C$ *J*-couplings show a larger error in some cases due to their smaller magnitudes. In all cases, experimental couplings are larger in the protonated (neutral) form than the ionized form, and this trend is reproduced in the calculated couplings. The sources of error cannot be identified easily, especially since $^{1}J_{CH}$, $^{1}J_{CC}$ and $^{2}J_{CC}$ in saccharides are very sensitive to exocyclic C−O bond conformations involving one or more carbons within the coupling pathways. In the present work, no attempt was made to take this C−O contribution into account quantitatively, since the dynamics of these conformational fluctuations in solution cannot be modeled reliably at present. This factor must be taken into account in any effort to strictly assess the accuracy of DFT-calculated *J*-couplings (and other NMR properties) in saccharides.

Table 10. Summary of *J*-Couplings That Differ in Methyl Glucopyranuronides 2/3 and Methyl Glucopyranosides 4/5

J-coupling	observed effect
$^{1}J_{C4,H4}$	1−3 Hz larger in **2**/**3**
$^{1}J_{C5,H5}$	3−6 Hz larger in **2**/**3**
$^{2}J_{C4,H5}$	∼1 Hz more negative in **2**/**3**
$^{2}J_{C5,H4}$	∼0.6 Hz more positive in **2**/**3**
$^{2}J_{C6,H5}$	∼2.5 Hz more neqative in **2**/**3**
$^{3}J_{C6,H4}$	∼1 Hz smaller in **2**/**3**
$^{1}J_{C4,C5}$	∼2 Hz smaller in **2**/**3**
$^{1}J_{C5,C6}$	∼18 Hz larger in **2**/**3**
$^{2}J_{C3,C5}$	Smaller or larger (<1.3 Hz) in **2**/**3** depending on ionization state
$^{2}J_{C4,C6}$	∼ 1 Hz more negative in **2**/**3**
$^{3}J_{C1,C6}$	∼ 1 Hz larger in **2**/**3**
$^{3}J_{C3,C6}$	∼ 1 Hz larger in **2**/**3**

DFT calculations show relatively free rotation about the C5−C6 bond in aldohexopyranuronides in solution (energy barriers <4−5 kcal/mol) in two C4−O4 bond conformations (θ = 60° and 180°). This rotational barrier increases significantly for θ = −60°, presumably due to the stabilizing effect of intramolecular H-bonding. Whether this enhanced barrier exists in solution is unclear. For the protonated (neutral) forms, the preferred C5−C6 bond conformation orients the carboxyl plane nearly orthogonal to the C5−H5 bond (Schemes S1 and S2, Supporting Information), whereas in the ionized form, the carboxyl plane is either parallel to the C5−O5 bond or to the C5−H5 bond. In the crystal structure[32], the C4−C5−C6−O6 torsion angles are ∼90° and ∼−90°, that is, the carboxylate plane is orthogonal to the C4−C5 bond. This geometry can be viewed as intermediate between those predicted by DFT for the ionized state (Scheme S3, Supporting Information). In the X-ray structure, however, a sodium ion bridges one of the carboxylate oxygens and the ring oxygen, thus anchoring the C5−C6 bond torsion. Therefore, the preferred C5−C6 bond conformation in the crystal does not necessarily reflect its intrinsic conformational properties in solution.

DFT calculations show that several *J*-couplings are sensitive to C5−C6 bond rotation (ω). These couplings include $^{1}J_{C5,H5}$, $^{2}J_{C4,H5}$, and $^{1}J_{C4,C5}$. Contrary to expectation, $^{1}J_{C5,C6}$ is only slightly affected by this rotation.

Prior work on the use of NMR *J*-couplings to investigate *O*-glycoside linkage conformation in oligo/polysaccharides focused primarily on *J*-couplings residing on the donor side of the linkage (e.g., the left residue in Scheme 1).[12−14] Generally, six couplings are employed: $^{2}J_{C1',C4}$, $^{3}J_{C2',C4}$ and

dx.doi.org/10.1021/jo3011182 | J. Org. Chem. 2012, 77, 9521−9534

Table 11. Comparison of Experimental and Calculated (DFT) *J*-Couplings in the Protonated and Ionized Forms of 2 and 3

J-coupling	pD 2.0, NMR	pD 2.0, DFT	pD 2.0, difference[a]	pD 7.0, NMR	pD 7.0, DFT	pD 7.0, difference
$^{1}J_{C1,H1}$ (2)	171.4	176.6	−5.2 (2.9)[b]	170.6	171.7	−1.1 (0.6)
$^{1}J_{C1,H1}$ (3)	162.4	169.3	−6.9 (4.1)	161.5	165.8	−4.3 (2.6)
$^{1}J_{C4,H4}$ (2)	146.0	151.5	−5.5 (3.6)	145.2	149.1	−3.9 (2.6)
$^{1}J_{C4,H4}$ (3)	147.8	151.9	−4.1 (2.7)	146.8	149.8	−3.0 (2.0)
$^{1}J_{C5,H5}$ (2)	150.3	151.9	−1.6 (1.1)	147.7	147.4	0.3 (−0.2)
$^{1}J_{C5,H5}$ (3)	147.2	149.8	−2.6 (1.7)	144.2	145.0	−0.8 (0.6)
$^{1}J_{C5,C6}$ (2)	64.1	65.4	−1.3 (2.0)	59.1	61.3	−2.2 (3.6)
$^{1}J_{C5,C6}$ (3)	64.2	65.4	−1.2 (1.8)	59.0	61.5	−2.5 (4.1)
$^{2}J_{C3,C5}$ (2)	+1.9	+2.6	−0.7 (27)	+0.9	+1.4	−0.5 (36)
$^{2}J_{C3,C5}$ (3)	+2.8	+3.4	−0.6 (18)	+1.8	+1.9	−0.1 (5.3)

[a]Defined as the experimental (NMR) *J*-coupling − calculated (DFT) *J*-coupling; all values in the table are in Hz. [b]Values in parentheses are percent errors, calculated from difference/DFT value × 100.

$^{3}J_{H1',C4}$ sensitive to ϕ, and $^{3}J_{C1',H4}$, $^{3}J_{C1',C3}$ and $^{3}J_{C1',C5}$ sensitive to ψ.[12] Recent work has suggested that $^{2}J_{C2',H1'}$ may also be useful to evaluate ϕ.[23] Using model structure **10**$_c$, five *J*-couplings on the acceptor side of the linkage were examined as probes of ψ in β-(1→4)-linkages, namely, $^{1}J_{C3,C4}$, $^{1}J_{C4,C5}$, $^{2}J_{C3,C5}$, $^{3}J_{C4,H4}$, and $^{3}J_{C5,H4}$. These couplings exhibited a discernible dependence on ψ, but in some cases also showed a dependency on ω (i.e., those couplings involving C5). The latter couplings might possibly be parametrized in both ϕ and ω, allowing an appraisal of correlated conformation about both bonds similar to that described for exocyclic hydroxymethyl groups in aldohexopyranosyl rings.[16] Additional study of these potential correlations might prove beneficial since the present 3−4 couplings per *O*-glycosidic linkage torsion limits the ability to discriminate between potential linkage conformational models based solely on the interpretation of experimental couplings. Increasing the ensemble of *J*-couplings sensitive to a given bond torsion in an *O*-glycosidic linkage increases redundancy and may permit more detailed assignments of linkage conformation.

In summary, NMR studies of the methyl glycosides of D-glucopyranuronic acid have revealed systematic changes in $^{1}H-^{1}H$, $^{13}C-^{1}H$ and $^{13}C-^{13}C$ spin-couplings, and ^{1}H and ^{13}C chemical shifts, as a function of anomeric configuration, COOH ionization state, and C5 substitution (CH_2OH vs COOH/COO^-). The observed changes are largely independent of changes in ring conformation. Quantification of these effects in structurally and conformationally defined monosaccharides having the *gluco* configuration provides important reference data for anticipated structural studies of other uronic acid monosaccharides, and of uronic acid-containing biomolecules, especially those that are conformationally flexible due to their uronic acid constituents (e.g., hyaluronic acid).

EXPERIMENTAL METHODS

A. Reagents. D-[1-^{13}C], [2-^{13}C], [3-^{13}C], [4-^{13}C], [5-^{13}C] and [6-^{13}C]glucose were obtained from Omicron Biochemicals, Inc. (South Bend, IN).

B. Synthesis of ^{13}C-Labeled Methyl D-Glucopyranosiduronides. The synthetic route used to prepare [1-^{13}C]**2** and [1-^{13}C]**3** is shown in Scheme 2; the same pathway was used to prepare the remaining 10 ^{13}C-isotopomers.

The general synthetic protocol was similar to that described for the preparation of D-penturonic acids.[15,36] Singly ^{13}C-labeled D-glucose (2.02 g, 11.2 mmol) was dissolved in anhydrous methanol (150 mL), dry Dowex 50WX8 (200−400 mesh) (H^+) ion-exchange resin (2.0 g) was added, and the suspension was refluxed for 36 h. After filtration to remove the resin, the solution was concentrated at 30 °C *in vacuo* to dryness, the residue was dissolved in a minimum volume of distilled water, and the solution was applied to a column (2.5 cm × 50 cm) of Dowex 1 × 8 (200−400 mesh) anion-exchange resin in the OH^- form.[15,18,37] The column was eluted with distilled, decarbonated water (1.0 mL/min), and fractions (18 mL) were collected and assayed by TLC (silica gel; spots detected by charring after spraying with 1% (*w*/*v*) $CeSO_4$−2.5% (*w*/*v*) $(NH_4)_6Mo_7O_{24}$−10% aq H_2SO_4 reagent).[38] Aldohexofuranosides bound more strongly to the resin than aldohexopyranosides, and unreacted D-glucose (if present) did not elute. Fractions containing the glucopyranosides were pooled and evaporated to dryness at 30 °C *in vacuo* to give methyl α-D-[^{13}C]glucopyranoside (fractions 17−23) and methyl β-D-[^{13}C]glucopyranoside (fractions 27−34), which were identified by ^{13}C NMR[39] and crystallized from methanol.

Methyl α-D-[^{13}C]glucopyranoside or methyl β-D-[^{13}C]-glucopyranoside (0.97 g, 5.0 mmol) was dissolved in distilled water (100 mL, pH ∼7.5), and sodium bicarbonate (100 mg) was added to adjust the solution pH to 8.4. To this solution was added 5% platinum on activated carbon catalyst (Pt/C; 300 mg) that had been prereduced with hydrogen. After the air in the reaction flask was purged and replaced with O_2, the reaction flask was partially immersed in an oil bath at 50 °C and the mixture was stirred (bar magnet) for 15 h. During this period, the solution pH was maintained above 7 with occasional additions of solid sodium bicarbonate. After catalyst removal by vacuum filtration, the reaction mixture was applied to a column (2.5 cm × 30 cm) of DEAE-Sephadex A-25 anion-exchange resin in the bicarbonate form, and the column was eluted with a 2000-mL linear gradient (0.02−0.07 M) of sodium bicarbonate at a flow rate of 1.0 mL/min. Fractions (18 mL) were collected and assayed by TLC (see above). Fractions 67−99 containing the uronide were pooled and concentrated at 30 °C *in vacuo* to ∼10 mL. This solution was treated batchwise with excess Dowex HCR-W2 (H^+) ion-exchange resin, the resin was removed by filtration, and the filtrate was frozen and lyophilized. Yields from the Pt oxidation reactions were ∼50% based on weights of the lyophilized product.

C. NMR Spectroscopy. Solutions of ^{13}C-labeled uronides were prepared at different solution pD (pH meter reading on the $^{2}H_2O$ solution after calibration with standard buffers) by dissolving samples in $^{2}H_2O$ and adjusting the solution pD with NaOD or with batchwise addition of Dowex HCR-W2 (H^+) (16−40 mesh) ion-exchange resin. Solutions (∼300 μL, ∼0.1 M) were transferred to 3-mm NMR tubes prior to analysis. High-resolution 1D ^{1}H and $^{13}C\{^{1}H\}$ NMR spectra were obtained at 30 °C on a 600-MHz FT-NMR spectrometer equipped with a 3-mm $^{13}C/^{1}H$ microprobe. In some cases, 1D ^{1}H NMR spectra were recollected on a 300-MHz FT-NMR spectrometer to reduce or eliminate non-first-order effects typically caused by the overlap of 1/2 of a ^{1}H signal split by $^{1}J_{CH}$ with another signal. 600-MHz ^{1}H NMR spectra were collected with a 2100 Hz spectral window and a ∼4.0 s recycle time. $^{13}C\{^{1}H\}$ NMR spectra (150 MHz) were collected with an ∼28 000 Hz spectral window and an ∼5.5 s recycle time. FIDs were zero-filled once or twice to give final digital resolutions of <0.05 Hz/pt, and FIDs were processed with resolution enhancement (Gaussian or sine-bell functions) to improve spectral resolution and

dx.doi.org/10.1021/jo3011182 | J. Org. Chem. 2012, 77, 9521−9534

Scheme 2

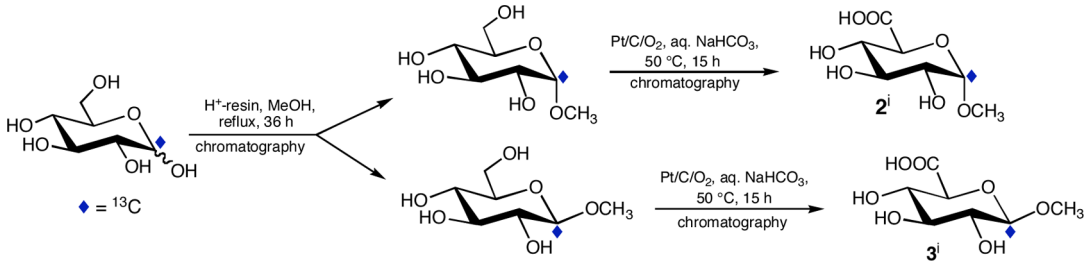

facilitate the measurement of smaller *J*-couplings. The degree of enhancement was chosen empirically based on the observed effects on line shape and spectral S/N. Chemical shifts were referenced externally to sodium 4,4-dimethyl-4-silapentane-1-sulfonate (DSS). When necessary (non-first-order behavior), ^{1}H NMR spectra were simulated with MacNUTs[17] to extract accurate chemical shifts and *J*-couplings.

CALCULATIONAL METHODS

A. Selection and Geometric Optimization of Model Structures. Native (i.e., fully substituted) structures of the protonated and ionized forms of **2** and **3** in the $^4C_1$ ring conformation were chosen for theoretical studies of energies and *J*-couplings. Throughout the manuscript, calculated structures are denoted $\mathbf{2}_c^P$, $\mathbf{2}_c^i$, $\mathbf{3}_c^P$ and $\mathbf{3}_c^i$ to distinguish them from experimental compounds $\mathbf{2}^P$, $\mathbf{2}^i$, $\mathbf{3}^P$ and $\mathbf{3}^i$, respectively, where the "c" subscript denotes a calculated structure and the "p" or "i" superscript denotes the protonated and ionized form, respectively. Density functional theory (DFT) calculations were conducted within *Gaussian*03[40] using the B3LYP functional[41] and 6-31G* basis set[42] for geometric optimization, as described previously.[43,44] These calculations included the effects of solvent water, which were treated using the Self-Consistent Reaction Field (SCRF)[45] and the Integral Equation Formalism (polarizable continuum) model (IEFPCM)[46] as implemented in *Gaussian*03. Three C−O bond torsion angles, C2−C1−O1−CH_3, C3−C2−O2−H and C4−C3−O3−H, were fixed at 180° in all calculations. The fourth C−O bond torsion, C5−C4−O4−H (denoted θ), was either fixed at 60°, 180°, −60°, or set initially at these angles and allowed to optimize during the calculations, yielding two sets of 36 optimized structures. Only the former data set (fixed θ) were used to calculate *J*-couplings (see below). The C4−C5−C6−O6 torsion angle (denoted ω where O6 is the *protonated* O6 in the COOH forms $\mathbf{2}_c^P$ and $\mathbf{3}_c^P$) was rotated systematically in fixed 30° increments through 360° while all remaining geometric parameters were optimized except those identified above.

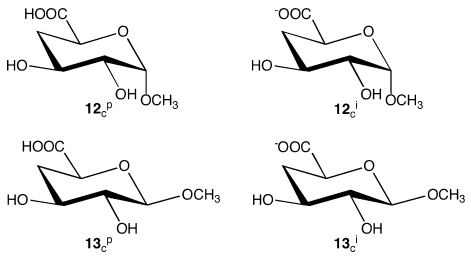

Solvated DFT calculations were also conducted on model structures $\mathbf{10}_c^P$, $\mathbf{10}_c^i$, $\mathbf{12}_c^P$, $\mathbf{12}_c^i$, $\mathbf{13}_c^P$ and $\mathbf{13}_c^i$ using the same set of exocyclic C−O torsional constraints used for $\mathbf{2}_c^P$, $\mathbf{2}_c^i$, $\mathbf{3}_c^P$ and $\mathbf{3}_c^i$. In the calculations on $\mathbf{10}_c^P$ and $\mathbf{10}_c^i$, the C5−C4−O4−CH_3 torsion angle was fixed at 60°, 180° and −60°, giving 36 optimized structures in each case. For $\mathbf{12}_c$ and $\mathbf{13}_c$, 12 optimized structures on each structure were obtained from 30° rotations about ω.

B. DFT Calculations of NMR Spin-Coupling Constants. J_{HH}, J_{CH} and J_{CC} spin-couplings were calculated in $\mathbf{2}_c^P$, $\mathbf{2}_c^i$, $\mathbf{3}_c^P$, $\mathbf{3}_c^i$, $\mathbf{10}_c^P$ and $\mathbf{10}_c^i$ using *Gaussian*03[40] and DFT (B3LYP).[41] The Fermi contact,[47−49] diamagnetic and paramagnetic spin−orbit, and spin-dipole terms[47] were recovered using a [5s2p1d|3s1p] basis set,[50] and raw (unscaled) calculated couplings are reported; these values have a estimated error of ∼5% based on prior analyses.[50] *J*-Coupling calculations included the effects of solvent water, which were treated using the Self-Consistent Reaction Field (SCRF)[45] and the Integral Equation Formalism (polarizable continuum) model (IEFPCM)[46] as implemented in *Gaussian*03. Three data sets with the C5−C4−O4−H torsion angle fixed at 60°, 180° and −60° were used to calculate *J*-couplings in $\mathbf{2}_c^P$, $\mathbf{2}_c^i$, $\mathbf{3}_c^i$, $\mathbf{10}_c^P$ and $\mathbf{10}_c^i$ ($12\omega \times 3\theta = 36$ structures/*J*).

ASSOCIATED CONTENT

Supporting Information

Supplemental tables, figures, and schemes; complete ref 40. This material is available free of charge via the Internet at http://pubs.acs.org.

AUTHOR INFORMATION

Corresponding Author

*aseriann@nd.edu

Present Address

‡Department of Chemistry, School of Science, Wuhan University of Technology, Wuhan, 430070, China

Notes

The authors declare no competing financial interest.

ACKNOWLEDGMENTS

This work was supported by a grant from the National Institutes of Health (GM59239) (to A.S.). The Notre Dame Radiation Laboratory is supported by the Office of Basic Energy Sciences of the United States Department of Energy. This is Document No. NDRL-4901 from the Notre Dame Radiation Laboratory.

REFERENCES

(1) Alkins, E. D.; Sheehan, J. K. *Nat. New Biol.* **1972**, *235*, 253−254.
(2) Chakrabarti, B.; Park, J. W. *CRC Crit. Rev. Biochem.* **1980**, *8*, 225−313.
(3) San Antonio, J. D.; Iozzo, R. V. *Encyclopedia of Life Sciences*; Wiley: New York, 2001; pp 1−8.
(4) Necas, J.; Bartosikova, L.; Brauner, P.; Kolar, J. *Vet. Med. (Prague, Czech Repub.)* **2008**, *53*, 397−411.
(5) Stern, R. *Eur. J. Cell. Biol.* **2004**, *83*, 317−25.
(6) (a) Basu, N. K.; Kole, L.; Basu, M.; Chakraborty, K.; Mitra, P. S.; Owens, I. S. *J. Biol. Chem.* **2008**, *283*, 23048−23061. (b) Banerjee, R.; Pennington, M. W.; Garza, A.; Owens, I. S. *Biochemistry* **2008**, *47*, 7385−7392.
(7) (a) Smirnoff, N. *Vitam. Horm. (London, U.K.)* **2001**, *61*, 241−266. (b) Linster, C. L.; Van Schaftingen, E. *FEBS J.* **2006**, *273*, 1516−1527.
(8) King, C.; Rios, G.; Green, M.; Tephly, T. *Curr. Drug Metab.* **2000**, *1*, 143−61.
(9) Jaques, L. W.; Macaskill, J. B.; Weltner, W. *J. Phys. Chem.* **1979**, *83*, 1412−1421.
(10) Amemura, A.; Hisamatsu, M.; Ghai, S. K.; Harada, T. *Carbohydr. Res.* **1981**, *91*, 59−65.

(11) Klepach, T.; Zhang, W.; Carmichael, I.; Serianni, A. S. *J. Org. Chem.* **2008**, *73*, 4376−4387.
(12) Bose, B.; Zhao, S.; Stenutz, R.; Cloran, F.; Bondo, P. B.; Bondo, G.; Hertz, B.; Carmichael, I.; Serianni, A. S. *J. Am. Chem. Soc.* **1998**, *120*, 11158−11173.
(13) Cloran, F.; Carmichael, I.; Serianni, A. S. *J. Am. Chem. Soc.* **1999**, *121*, 9843−9851.
(14) Olsson, U.; Serianni, A. S.; Stenutz, R. *J. Phys. Chem.* **2008**, *112*, 4447−4453.
(15) Wu, J.; Serianni, A. S. *Carbohydr. Res.* **1991**, *210*, 51−70.
(16) Thibaudeau, C.; Stenutz, R.; Hertz, B.; Klepach, T.; Zhao, S.; Wu, Q.; Carmichael, I.; Serianni, A. S. *J. Am. Chem. Soc.* **2004**, *126*, 15668−15685.
(17) *MacNUTs Pro*; Acorn NMR Inc.: Livermore, CA.
(18) Podlasek, C. A.; Wu, J.; Stripe, W. A.; Bondo, P. B.; Serianni, A. S. *J. Am. Chem. Soc.* **1995**, *117*, 8635−8644.
(19) Bock, K.; Lundt, I.; Pedersen, C. *Tetrahedron Lett.* **1973**, 1037.
(20) Bock, K.; Pedersen, C. *Acta Chem. Scand., Ser. B* **1975**, *B29*, 258.
(21) Church, T. J.; Carmichael, I.; Serianni, A. S. *J. Am. Chem. Soc.* **1997**, *119*, 8946−8964.
(22) Podlasek, C. A.; Stripe, W. A.; Carmichael, I.; Shang, M.; Basu, B.; Serianni, A. S. *J. Am. Chem. Soc.* **1996**, *118*, 1413−1425.
(23) Klepach, T. E.; Carmichael, I.; Serianni, A. S. *J. Am. Chem. Soc.* **2005**, *127*, 9781−9793.
(24) Bose-Basu, B.; Klepach, T.; Bondo, G.; Bondo, P. B.; Zhang, W.; Carmichael, I.; Serianni, A. S. *J. Org. Chem.* **2007**, *72*, 7511−7522.
(25) Klepach, T.; Carmichael, I.; Serianni, A. S. *J. Am. Chem. Soc.* **2008**, *130*, 11892−11900.
(26) Carmichael, I.; Chipman, D. M.; Podlasek, C. A.; Serianni, A. S. *J. Am. Chem. Soc.* **1993**, *115*, 10863−10870.
(27) Zhao, S.; Bondo, G.; Zajicek, J.; Serianni, A. S. *Carbohydr. Res.* **1998**, *309*, 145−152.
(28) Wu, J.; Bondo, P. B.; Vuorinen, T; Serianni, A. S. *J. Am. Chem. Soc.* **1992**, *114*, 3499−3505.
(29) Klepach, T.; Carmichael, I.; Serianni, A. S., unpublished results.
(30) Gooley, P. R.; Keniry, M. A.; Dimitrov, R. A.; Marsh, D. E.; Keizer, D. W.; Gayler, K. R.; Grant, B. R. *J. Biomol. NMR* **1998**, *12*, 523−534.
(31) Kouwijzer, M. L. C. E.; van Eijck, B. P.; Kooijman, H.; Kroon, J. *Acta Crystallogr.* **1995**, *B51*, 209−220.
(32) DeLucas, L. J.; Gartland, G. L.; Bugg, C. E. *Carbohydr. Res.* **1978**, *62*, 213.
(33) Whitfield, D. M.; Sarkar, B. *J. Inorg. Biochem.* **1991**, *41*, 157−170.
(34) Eykyn, T. R.; Kuchel, P. W. *Magn. Reson. Med.* **2003**, *50*, 693−696.
(35) Labotka, R. J.; Kleps, R. A. *Biochemistry* **1983**, *22*, 6089−6095.
(36) Mallat, T.; Baiker, A. *Catal. Today* **1994**, *19*, 247−284. (b) Wu, J.; Serianni, A. S.; Bondo, P. *Carbohydr. Res.* **1992**, *226*, 261−269.
(37) Austin, P. W.; Hardy, F. E.; Buchanan, J. C.; Baddiley, J. *J. Chem. Soc.* **1963**, 5350.
(38) Tropper, F. D.; Andersson, F. O.; Grant-Maitre, C.; Roy, R. *Carbohydr. Res.* **1992**, *229*, 149−154.
(39) Bock, K.; Pedersen, C. *Adv. Carbohydr. Chem. Biochem.* **1983**, *41*, 27−66.
(40) Frisch, M. J., et al. *Gaussian03*, Revision A.1; Gaussian, Inc.: Pittsburgh, PA, 2003.
(41) Becke, A. D. *J. Chem. Phys.* **1993**, *98*, 5648−5652.
(42) Hehre, W. J.; Ditchfield, R.; Pople, J. A. *J. Chem. Phys.* **1972**, *56*, 2257−2261.
(43) Cloran, F.; Zhu, Y.; Osborn, J.; Carmichael, I.; Serianni, A. S. *J. Am. Chem. Soc.* **2000**, *122*, 6435−6448.
(44) Cloran, F.; Carmichael, I.; Serianni, A. S. *J. Am. Chem. Soc.* **2001**, *123*, 4781−4791.
(45) Cancés, M. T.; Mennucci, B.; Tomasi, J. *J. Chem. Phys.* **1997**, *107*, 3032−3041.
(46) Cammi, R.; Mennucci, B.; Tomasi, J. *J. Phys. Chem.* **2000**, *104A*, 5631−5637.
(47) Sychrovský, V.; Gräfenstein, J.; Cremer, D. *J. Chem. Phys.* **2000**, *113*, 3530−3547.
(48) Helgaker, T.; Watson, M.; Handy, N. C. *J. Chem. Phys.* **2000**, *113*, 9402−9409.
(49) Barone, V.; Peralta, J. E.; Contreras, R. H.; Snyder, J. P. *J. Phys. Chem. A* **2002**, *106*, 5607−5612.
(50) Stenutz, R.; Carmichael, I.; Widmalm, G.; Serianni, A. S. *J. Org. Chem.* **2002**, *67*, 949−958.